Use and Evaluation of Atmospheric Stability Products derived from the NOAA Unique Cross-track Infrared Sounder (CrIS)/Advanced Technology Microwave Sounder (ATMS) Processing System (NUCAPS) Retrieval Products

Silvia Regina Santos da Silva

A scholarly paper in partial fulfillment of the requirements for the degree of

Master of Science

April 2016

Department of Atmospheric and Oceanic Science, University of Maryland
College Park, Maryland

Research Advisor: Dr. Flavio Iturbide-Sanchez (NOAA/NESDIS)

Academic Advisor: Dr. Ning Zeng

Table of Contents

Abstract

The National Oceanic and Atmospheric Administration (NOAA) Unique Cross-track Infrared Sounder (CrIS)/Advanced Technology Microwave Sounder (ATMS) Processing System (NUCAPS) is the official NOAA system retrieving atmospheric vertical temperature and moisture profiles (AVTPs and AVMPs) from CrIS and ATMS measurements. Both state-of-the-art instruments are currently onboard the Suomi National Polar-orbiting Partnership (S-NPP) spacecraft, launched on October 28th 2011, as part of the Joint Polar Satellite System (JPSS). This study investigates the performance of atmospheric stability indices and parameters (SIPs) computed from NUCAPS AVTPs and AVMPs in order to verify their overall quality and applicability to the operational meteorological routine. The methodology considered comparisons between conventional and dedicated/reference radiosonde observations (RAOBs) with the closest NUCAPS retrievals and analysis profiles from the European Centre for Medium-Range Weather Forecasts (ECMWF) global model, collocated within a maximum radius of 50 km and ±1-hr time difference. Parameters evaluated include Total Precipitable Water, Lifted Index, K-Index, Total-Totals Index, as well as the recently developed Galvez-Davison Index, optimized for the tropics. The SIPs were computed from each of the three sources of soundings, NUCAPS, RAOBs, and ECMWF, and intercompared with proper metrics. Evaluation is divided by latitudinal bands, mid-latitudes (60N to 30N) and tropics (30N to 30S), covering a very comprehensive sample of RAOBs resulting in approximately 10000 for the mid-latitudes case, and ~3700 for the tropics. Among all parameters examined, NUCAPS derived TPW exhibited the highest level of statistical agreement with RAOB counterparts. The remaining NUCAPS SIPs exhibited good to intermediate

4

levels of agreement with their RAOBs derived versions, with the caveat that these parameters tended to be underestimates of RAOBs, particularly over the range of values associated with unstable atmospheric conditions. A noteworthy finding is that NUCAPS resolved very well the mean lowest 100-hPa thermal/moisture characteristics. Comparison results over severe weather cases demonstrated NUCAPS capability of generating reliable fields of atmospheric stability, identifying areas under unstable atmospheric conditions, as well as capturing synoptic-scale convective signatures. Thus, NUCAPS stability products are proposed to be additional and complementary tools for short-term forecasting.

Acknowledgements

The Master of Science degree from the University of Maryland is a significant accomplishment for me and I am indebted to many individuals and institutions that directly or indirectly helped me achieving it.

First I would like to thank the financial support received from the CAPES Foundation/Ministry of Education of Brazil under grant 88888.075925/2013-00, and the initiative of the Brazilian Government of creating the Brazilian Scientific Mobility Program. Also, my academic advisor Dr. Ning Zeng for the opportunity of being admitted in the program, and advices throughout my academic life. Those provided me encouragement, especially at the beginning of the course.

Another priceless guidance came from my research advisor Dr. Flavio Iurbide-Sanchez, who gave me unconditional support during the progress of this study and also valuable advices from his personal experience to succeed in the program. His support involved many aspects of solving the scientific questions (and also problems!) the work required, as well as sharing his knowledge of the subject. But the most important support was his constant motivation and belief in the potential of this study. I am also grateful to Mr. Kenneth Pryor from NOAA/NESDIS for his positive feedback and comments with respect to this work.

Additionally, I would like to thank the Federal University of Rio de Janeiro and the Brazilian Navy (and obviously all their members), which provided me the essential background to overcome the rigorous requirements of the graduate program of the AOSC Department. These institutions built most of what I am today! Thanks also to all the

faculty members of the AOSC Department, in special the ones that I took courses with, who shared their valuable expertise, challenged me and showed that every day is an opportunity of constant learning and growing in the atmospheric sciences field. Moreover, Dr. Sumant Nigam and Dr. Alfredo Ruiz-Barradas for opening opportunities for new learning experiences. Dr. Rachel Pinker, who I have been working with as a Teaching Assistant, for her example of professionalism and companionship. Thanks also to the administrative and supporting personnel of the AOSC Department (Jeff, Tammy, Bernadette, June and Tameka), always very helpful. My colleagues Agniv, Vitally, Dolly Hall, Meredith Nichols and Daniel Nielsen from the Fall 2014 class, who also helped me in many moments, but also for the talks. All my dear friends from Brazil, in special Eliana, Shirley, Fabiane, Caruzzo, Rodrigo and Pristo, who have constantly sent me support and encouragement to proceed. And finally my loved family, in special my brother Nelson and my mother, who I miss very much, for having tolerated my many and long moments of absence and for all they have done for me throughout my life.

I would still have to thank more people, but for the sake of space I will have to stop here. However I am really thankful to all that helped me in any aspect. All of you are responsible for this achievement. Thank you.

List of Tables

List of Figures

Chapter 1. Introduction

For several decades, atmospheric stability indices (SIs) computed from operational radiosonde profiles have been routinely used by weather forecasters to identify convective unstable environments that can potentially lead to thunderstorms development and their consequent hazards, such as heavy rain, strong wind gusts, hail, lightning, and even tornadoes. With the advent and deployment of sophisticated sounding instruments aboard environmental satellites, and the development of retrieval algorithms using infrared (IR) and microwave (MW) observations, high-quality atmospheric vertical temperature and moisture profiles (AVTPs and AVMPs) have became available showing potential for thermodynamic analysis. In this paper, AVTPs and AVMPs generated by the National Oceanic and Atmospheric Administration (NOAA) Unique Cross-track Infrared Sounder (CrIS)/Advanced Technology Microwave Sounder (ATMS) Processing System (NUCAPS) were used to derive an ensemble of atmospheric stability indices and parameters (SIPs) of interest for operational weather forecasting.

Both CrIS and ATMS are currently on board the Suomi National Polar-orbiting Partnership (S-NPP) spacecraft, launched on October 28th 2011 as part of the Joint Polar Satellite System (JPSS), the U.S. polar-orbiting operational satellite mission planned to be the successor to the Polar-Orbiting Environmental Satellites (POES) program. Hence, the JPSS mission is going to ensure continuity of critical environmental observations in the early afternoon orbit. The S-NPP was the first satellite in the JPSS program with the specific missions of providing on-orbit testing, calibration, and validation of sensors, algorithms, ground-based operations and data processing systems prior to the launch of

JPSS-1, as well as anticipating the access and evaluation of data from JPSS sensors (Lee *et al.*, 2010). Its follow-on, JPSS-1, is scheduled for launching in 2017 (Goldberg *et al.*, 2013). The entire cycle for the JPSS series will be completed by the JPSS-2, JPSS-3 and JPSS-4 satellites. Like S-NPP, the future JPSS payloads were conceived to include similar CrIS and ATMS instruments, as well as the Visible Infrared Imaging Radiometer Suite (VIIRS), and the Ozone Mapping and Profiler Suite (OMPS).

The NUCAPS S-NPP version 1.5 (henceforth NUCAPS) SIPs are compared with corresponding values derived from radiosonde observations (RAOBs), with the purpose of evaluating the retrieval ability to assess atmospheric stability, as well as better informing short-term forecasters and the scientific community. Additionally, SIPs computed from vertical profiles obtained from analyses fields of the European Centre for Medium-Range Weather Forecasts (ECMWF) global model are compared with RAOBs SIPs to obtain a secondary reference for NUCAPS performance, given the high level of skill achieved by the outputs of the ECMWF numerical prediction model (Bauer *et al.*, 2015).

As previously mentioned, this study aims to objectively assess the impact of using NUCAPS vertical profiles for the computation of SIPs, verifying their overall applicability as additional tools in the operational weather forecasting routine. This is an important study for potential users since, to the best of my knowledge, a similar research was never attempted using NUCAPS AVTP and AVMP products. In this respect, the usage of NUCAPS offers the advantage of increasing the spatial (e.g., data sparse regions; locations between RAOB stations) and temporal (e.g., profiles available between balloon launch

times) resolution of vertical temperature and moisture profiles necessary for the atmospheric stability evaluation.

Previous applications of satellite-derived SIPs have been reported in the literature. Some important contributions were inherited from the Geostationary Operational Environmental Satellite (GOES) sounders. Early works used the 12-channel Visible Infrared Spin Scan Radiometer (VISSR) Atmospheric Sounder (VAS) (Hayden, 1988). Some VAS derived parameters like the Total Precipitable Water (TPW), Total Totals index (TT) and Lifted index (LI), were applied to the analysis of preconvective environments (Smith *et al*., 1985; Chesters *et al*., 1986; Mostek *et al*., 1986). From that point, there has been a constant evolution of GOES sounders and retrieval algorithms until the current GOES 13-15 series, with 18 IR spectral bands to profile the atmosphere. This has allowed more accurate thermodynamic profiles and has increased nominal spatial and temporal resolution (currently hourly frequency) of derived stability products (Menzel *et al*., 1998, Dostalek and Schmit, 2001; Schmit *et al*., 2002, Li *et al*., 2008). Airmass parameters were also derived from vertical profiles generated by the Spinning Enhanced Visible and Infrared Imager (SEVIRI), onboard the Meteosat Second Generation (MSG) satellites - the geostationary satellites operated by the European Organisation for the Exploitation of Meteorological Satellites (EUMETSAT). Koenig and de Coning (2009) describe the physical retrieval method developed and its application to the SEVIRI instrument to derive the LI, TPW and the K-Index (KI). The MSG SEVIRI channels used by the physical retrieval algorithm were: three longwave radiation window channels (8.7, 10.8, and 12.0 µm), two water vapor channels (6.2 and 7.3 µm), and the

CO$_2$ channel (13.4 µm). On their work, Koenig and de Coning (2009) show the potential of using the EUMETSAT stability products as an aid forecasting tool for nowcasting, which was assessed through qualitative analysis of selected cases and objective evaluation using the occurrence of lightning as an indicator of severe convection.

Despite continuous progress, the usage of multi-channel sounders data from geostationary satellites suffer constraints due to limited spectral resolution and availability of retrieved profiles generally under clear-sky conditions. Efforts towards obtaining retrieved profiles from IR sounder measurements under cloudy conditions have been done. As an example, Li *et al*. (2009) applied a regression-based cloudy retrieval algorithm to GOES 12 sounder radiance measurements, focusing on thin and low thick cloud conditions. This approach, which included hourly surface observations and the National Center for Environmental Prediction (NCEP) Global Forecast System (GFS) forecast profiles as predictors, showed similar quality of the retrievals of moisture under clear and thin cloud conditions. In this context, JPSS polar-orbiting satellites offer added capabilities in relation to geostationary satellites due to the existence of the ATMS, a passive microwave sensor. The operation of the ATMS, collecting surface and atmospheric MW radiances even over cloudy conditions, in conjunction with the high spectral information provided by the IR hyperspectral sounder CrIS (1305 channels at nominal spectral resolution and 2211 channels at full spectral resolution) constitutes one of the key advancements achieved by this generation of satellites. By the processing of CrIS/ATMS measurements, NUCAPS delivers AVTP and AVMP products under clear, partly cloudy and cloudy scenes. The extent to which NUCAPS AVTPs and AVMPs add

15

information on the assessment of the atmospheric stability is objectively verified in this paper.

The paper is organized as follows: Chapter 2 summarizes the sounding instruments and the NUCAPS retrieval system; Chapter 3 briefly reviews the background on Atmospheric Stability and SIs; Chapter 4 describes the methodology and data sets used herein; Chapter 5 presents the results after the evaluation of the NUCAPS AVTPs and AVMPs over selected geographic domains; Chapter 6 shows results about the statistical evaluation of the NUCAPS SIPs; Chapter 7 presents the performance of the use of NUCAPS-based SIs over two case studies where severe weather conditions were identified, and Chapter 8 is dedicated to provide the conclusions of this work.

Chapter 2. The NOAA Unique Cross-track Infrared Sounder (CrIS)/Advanced Technology Microwave Sounder (ATMS) Processing System (NUCAPS)

This chapter provides a brief description of the CrIS and ATMS sounding sensors onboard the S-NPP satellite. This is followed by an overview of the NUCAPS Retrieval System.

2.1 Advanced Technology Microwave Sounder (ATMS)

The ATMS is a cross-track scanner radiometer with 22 channels covering four MW spectral bands: K (23.8GHz)/Ka (31.4GHz), V (50.3–57.3GHz), W (88.2GHz), and G (165–183GHz). Table 1 provides a summary of the ATMS channel characteristics.

The ATMS was devised to have most of the sounding channels from its predecessors Advanced Microwave Sounding Unit-A1 (AMSU-A1), Unit-A2 (AMSU-A2), Unit-B (AMSU-B), and Microwave Humidity Sounder (MHS), operating on the POES-series satellites since the NOAA-15 (launched in 1998), or on the EUMETSAT Metop-A/Metop-B satellites (launched in 2006 and 2012, respectively), and also, on the National Aeronautics and Space Administration (NASA) Earth Observing System (EOS) Aqua platform (launched in 2002). However, the ATMS instrument counts with one additional temperature channel at 51.76 GHz, and two new water vapor sounding channels (19 and 21) to improve the thermodynamic characterization of the low to middle troposphere (Weng *et al*., 2012). As a result of the ATMS channel selection, channels 1-16 are primarily designed to profile the atmospheric temperature from the surface to about 1 hPa (~45 km), whereas channels 17-22 are designed for humidity soundings from

the surface to about 200 hPa (~15 km) (Weng *et al*., 2013). Further information regarding the instrument characteristics and calibration of the sensor can be found in Zou *et al*. (2013).

Table 1. ATMS Channel Spectral Characteristics.

Channel	Center Frequency (GHz)	Accuracy (K)	NEdT[a] @300 K (K)	Static Beamwidth (deg.)	Peak Weight Function[b] (hPa)
1	23.8	1	0.7	5.2	Window
2	31.4	1	0.8	5.2	Window
3	50.3	0.75	0.9	2.2	Window
4	51.76	0.75	0.7	2.2	950
5	52.8	0.75	0.7	2.2	850
6	53.596 ± 0.115	0.75	0.7	2.2	700
7	54.4	0.75	0.7	2.2	400
8	54.94	0.75	0.7	2.2	250
9	55.5	0.75	0.7	2.2	200
10	57.290344 (f_o)	0.75	0.75	2.2	100
11	f_o ± 0.217	0.75	1.2	2.2	50
12	f_o ± 0.3222 ± 0.048	0.75	1.2	2.2	25
13	f_o ± 0.3222 ± 0.022	0.75	1.5	2.2	10
14	f_o ± 0.3222 ± 0.010	0.75	2.4	2.2	5
15	f_o ± 0.3222 ± 0.0045	0.75	3.6	2.2	2
16	88.2	1	0.5	2.2	Window
17	165.5 ± 0.925	1	0.6	1.1	Window
18	183.31 ± 7	1	0.8	1.1	800
19	183.31 ± 4.5	1	0.8	1.1	700
20	183.31 ± 3	1	0.8	1.1	500
21	183.31 ± 1.8	1	0.8	1.1	400
22	183.31 ± 1	1	0.9	1.1	300

Sources: Goldberg et al. (2013); Weng et al. (2012).
[a]NEdT - Noise Equivalent Differential Temperature.
[b]Weighting Function Peaks at a US Standard Atmospheric Condition.

Another crucial advance lies on the larger ATMS scan angle of ± 52.725^o (± 48.3^o for AMSU-A) from the nadir direction. For all ATMS channels, measurements are taken every 1.11^o (angular sampling interval) at 96 Earth-viewing angles per scan line. This results in a wider swath width of ~2500 km. As a consequence, ATMS can operate without orbital gaps poleward of 20°, and shows increased coverage within the 20S-20N region (Weng *et al*., 2012). It should also be noted the better horizontal resolution of ATMS channels 3-16 of about 32 km at nadir (vs. about 47 km for the equivalent AMSU channels 3-15), as well as the high vertical resolution (3 to 6 km, approximately) of the temperature and moisture profiles derived from measurements of the ATMS channels 3-15 and 17-22, respectively (Goldberg *et al*., 2013; Weng *et al*. 2012). For ATMS channels 17-22, which have a beam size of 1.1 degrees, the horizontal resolution improves to nearly 16 km at nadir. Finally, the static beam width of 5.2 degrees for ATMS channels 1-2 leads to a footprint size close to 75 km at nadir. However, for purposes of processing by the NUCAPS, ATMS observations must be re-sampled to match the CrIS configuration scan geometry during the NUCAPS pre-processing step (Tan *et al*., 2015). In this step, the ATMS scan sets are basically synchronized with those of the CrIS instrument.

2.2 Cross-track Infrared Sounder (CrIS)

The Cross-track Infrared Sounder (CrIS) is a Fourier transform spectrometer with 1305 sounding channels, when operating at nominal spectral resolution, distributed among three IR spectral bands corresponding to longwave (LWIR: 9.14-15.38 µm),

midwave (MWIR: 5.71-8.26 µm), and shortwave (SWIR: 3.92-4.64 µm). Table 2 lists

key characteristics of the CrIS channels.

Table 2. CrIS Threshold Performance Characteristics Operating at Nominal Spectral Resolution.

Channel	Wavenumber (cm^{-1})	Spectral Resolution (cm^{-1})	Accuracy @ 287 K (%)	Maximum NEdN[a] (mW/ m^2 sr cm^{-1})	Nadir FOV (Km)
LWIR	650-1095	0.625	0.45	0.45 @ 670 cm^{-1} 0.15 @ 700 cm^{-1} 0.15 @ 850 cm^{-1} 0.15 @ 1050 cm^{-1}	14
MWIR	1210-1750	1.25	0.58	0.055 @ 1225 cm^{-1} 0.045 @ 1250 cm^{-1} 0.049 @ 1500 cm^{-1} 0.053 @ 1700 cm^{-1}	14
SWIR	2155-2550	2.5	0.77	0.0062 @ 2200 cm^{-1} 0.007 @ 2350 cm^{-1} 0.007 @ 2550 cm^{-1}	14

Source: JPSS program Level 1 Requirements Document (Supplement), version 2.10, June 25 2014, NOAA/NESDIS.
Available online: http://www.jpss.noaa.gov/pdf/L1RDS_JPSS_REQ_1002_NJO_v2.10_100914_final-1.pdf.
[a]NEdT - Noise Equivalent Differential Radiance.

CrIS is part of the recent generation of hyperspectral IR sounders that have caused

an unprecedented revolution in atmospheric sounding capability. Such generation of

advanced sounders also includes the Atmospheric Infrared Sounder (AIRS) on the Aqua

platform and the Infrared Atmospheric Sounding Interferometer (IASI) on board the

EUMETSAT Metop-A/Metop-B satellites. In common, these instruments possess highly

improved sounding capability due to their high spectral resolution and large number of

spectral channels. As shown in the work of Smith *et al*. (2009), the large number

(typically thousands of measurements) of noise independent spectral channels of radiance

provides an order of magnitude improvement in signal to noise ratio in comparison with

multi-spectral sounders (2 to 50 spectral channels). This study also demonstrated the improvement in sounding accuracy resulting from the hyperspectral resolution, which enables more precise spectral and radiometric calibration, reduces the impact of forward model errors, and enables the Earth's surface emissivity and cloud spectral properties to be more accurately accounted for during the retrieval process.

In particular, CrIS allows the derivations of vertical profiles of temperature and moisture with vertical resolution ranging between 1 to 2 km in the troposphere, and 3 to 5 km in the stratosphere (Goldberg *et al*., 2013). Recent studies have reported levels of radiometric uncertainty better than the requirements for the JPSS program (e.g., Tobin *et al*., 2013). Furthermore, CrIS offers the advantage of the lowest noise level in comparison to IASI and AIRS (Smith *et al*., 2015; Zavyalov *et al*., 2013).

Based on plane mirror interferometer technology, the CrIS instrument measures interferograms, which constitute the uncalibrated Raw Data Records (RDRs). RDRs are then converted to calibrated and geolocated radiance spectra, called Sensor Data Records (SDRs), by the ground processing system. For in-depth discussions of the CrIS interferometer, its measurement characteristics and the processing flow that enables the conversion of RDR into SDR products, the reader is referred to Han *et al*. (2013).

CrIS scanning geometry is based on a 2200 km swath width (full Earth view scan angle of +/-48.3^o). Each scan sweep occurs in the cross-track direction, in which CrIS measures a total of 30 fields of regard (FORs) along each scan line every 8s. For each of the three IR bands, one FOR consists of nine fields-of-view (FOVs), forming a 3 × 3 array of circles whose centers are separated by 1.1^o (~16 km at nadir). Since one FOV

21

corresponds to a nadir spatial resolution of about 14 km, a FOR corresponds to a footprint size of around 50 km at nadir (see Fig. 3 in Han *et al.*, 2013). Four scan lines of CrIS data define a granule, which constitute the basic unity for the delivery of data in near real time.

2.3 The NOAA Unique CrIS/ATMS Processing System (NUCAPS)

NUCAPS (Gambacorta *et al.*, 2014) is the official NOAA system retrieving vertical temperature, and water vapor profiles from the processing of CrIS and ATMS SDRs. These retrieval products are known as Environmental Data Records (EDRs). The suite of NUCAPS EDR products includes retrieved estimates of: (1) cloud fraction and cloud top pressure; (2) surface temperature and surface emissivity; and (3) atmospheric temperature, water vapor and trace gases vertical profiles (ozone, methane, carbon monoxide, carbon dioxide, nitrous oxide, nitric acid and sulfur dioxide).

The inversion algorithm is based upon the NASA AIRS Science Team Retrieval algorithm documented by Susskind *et al.* (2003; 2011) and was first implemented at NOAA in 2002 to process AIRS/AMSU data. Further development led to a code with a modular architecture capable of processing data from multiple sensors. This is done by the pre-processing of the SDRs into a common binary file format, which means that the input file to the retrieval code is rigorously the same. Hence, the same retrieval algorithm has been currently used at the NOAA National Environmental Satellite, Data, and Information Service (NESDIS) Center for Satellite Applications and Research to process the AIRS/AMSU suite, the IASI/AMSU/MHS suite (operational since 2008) and more recently the CrIS/ATMS suite (operational since 2014).

The use of ATMS/CrIS observations enables NUCAPS to retrieve AVTPs and AVMPs under non-precipitating conditions (clear, partly cloudy and cloudy). This is a key advantage with respect to retrieval algorithms processing solely IR radiances, strongly affected by clouds.

NUCAPS is described in detail in Gambacorta *et al*. (2014) and in the Algorithm Theoretical Basis Document (ATBD), available online at http://www.ospo.noaa.gov/Products/atmosphere/soundings/nucaps/docs/NUCAPS_ATBD_20130821.pdf. However for the sake of completeness, the six main modules of the system are recalled here: (1) a module dedicated to provide preliminary input data quality control, pre-process CrIS/ATMS observations, read the background climatology look up tables, and acquire the surface pressure from the GFS; (2) a MW retrieval module, which derives cloud liquid water flags and MW surface emissivity uncertainty (Rosenkranz, 2001); (3) a fast eigenvector regression retrieval module for temperature and moisture regression, trained using ECMWF analysis and CrIS all sky radiances (Goldberg *et al*., 2003); (4) a cloud clearing module that combines a set of MW and IR channels to produce cloud-cleared IR radiances (Chahine, 1974). The module support the use of visible observations provided by the onboard VIIRS instrument, ready for future aplications; (5) a second fast eigenvector regression retrieval module for the estimation of temperature and moisture using a regression trained against ECMWF analysis and CrIS cloud cleared radiances (Goldberg *et al*., 2003); and (6) a final IR/MW physical retrieval module, which employs the previous regression estimation as a first guess (Susskind *et al*., 2003). The final IR/MW retrieval module is based on an iterated regularized least

square minimization scheme in which an optimally selected subset of IR channels is used (Gambacorta and Barnet, 2013). This particular characteristic allows computational efficiency of the retrieval implementation in an operational environment. In this case, the CrIS spectrum at nominal spectral resolution, consisting of 1305 channels, is replaced by a subset of less than 500 channels. The sounding channel distribution is as follows: 24 for surface temperature and emissivity, 87 for temperature, 62 for water vapor, 53 for ozone, 27 for carbon monoxide, 54 for methane, 53 for carbon dioxide, 24 for nitrous oxide, 28 for nitric acid, and 24 for sulfur dioxide. As demonstrated by the study of Gambacorta and Barnet (2013), this channel selection constitutes the optimal subset capable of accounting for more than 99% of the total variance across the whole spectrum, except for the 600–700-cm^{-1} and 1700-cm^{-1} regions, where the explained variance is around 95%, and for the 2200–2300-cm^{-1} region, where the explained variance ranges between 85% and 99%.

The NUCAPS EDR products of AVTP and AVMP are operational products generated for fixed 100 pressure levels (1100 to 0.016 hPa). It is important to mention that for cloudy (cloud cover > 50%) and precipitating scenes, the IR/MW retrieval typically fails converging to a solution. In this work, all AVTPs and AVMPs profiles were derived from the IR/MW retrieval module. Since, each NUCAPS FOR is based upon 9 CrIS FOVs (one CrIS FOR), the horizontal resolution of the NUCAPS AVTPs and AVMPs varies along the CrIS scan line between 50 km at nadir to approximately 70×135 km at the scan edges.

Chapter 3. Atmospheric Stability and Stability Indices

The occurrence of atmospheric instability and the availability of moisture in the low- or mid-troposphere are two essential components to convective weather development. The existence of a triggering mechanism to provide the lifting of air parcels, until achieving the level of free convection (LFC) (above the LFC, parcels accelerate upward due to a positive buoyancy force), is a third contributor, particularly for deep convection development associated with severe weather (Peppler, 1988; Johns and Doswell, 1992). The study of atmospheric stability is anchored on the general concepts of static stability and the parcel method, evolving to related concepts of conditional, absolute, latent and potential/convective instability. These concepts are reviewed in Peppler (1988). In this context, most SIs were developed to provide an indication of the first two convective-generating mechanisms (individually or coupled) and constitute widely used tools among operational forecasters for very-short-range prediction (a few hours). However, users should be aware of the intended geographical region of application and purpose of each SI. Local objective performance evaluations providing proper thresholds and their seasonal variations must be performed for applications at different locations (Haklander and Van Delden, 2003; Koenig and de Coning, 2009). It is worth mentioning that it is beyond the scope of this paper to prove the forecasting skills of the SIPs included in this work or in general. This should be specifically addressed on the literature. The real impetus for this work is to determine the level of statistical agreement between RAOBs- and NUCAPS-derived SIPs in order to serve as an objective base of information on the skill of NUCAPS stability products in

25

relation to RAOBs, taken as the "truth" correlative measurements. Naturally, the concept of RAOBs as "truth" measurements implies the necessity of being mindful of limitations, such as their inherent error measurements of around 0.5K for temperature and 10% for relative humidity (Candlish *et al*., 2012).

The SIPs selected for this work are the most traditional parameters used by forecasters, except for the recently-developed GDI. They are briefly outlined below. In all cases, T and T_d correspond to the ambient air and dewpoint temperatures, respectively, and their numeric subscripts refer to the pressure levels they must be obtained from. The selection of SIPs also includes TPW, which is widely used to assess the potential for heavy precipitation at a location (typically associated with plumes of elevated TPW values). TPW (in mm) expresses the depth of liquid water accumulated at the surface if all the water vapor in a column of unit cross section extending from the surface to the top of the atmosphere were condensed and precipitated as rain.

3.1 Showalter Index (SWI)

The SWI (Showalter, 1953) is defined as:

$$SWI = T_{500} - T_{P,500} \tag{1}$$

where $T_{p,500}$ is the temperature of an air parcel lifted dry-adiabatically from 850 hPa to its lifting condensation level (LCL) and then moist-adiabatically to 500 hPa. The SWI was originally developed for applications in the southwestern U.S. related to the occurrence of non-severe convective showers and thunderstorms (Peppler, 1988). Negative values indicate increased potential for convective activity, especially with $SI \leq -3^o C$.

3.2 Lifted Index (LI)

The LI (Galway, 1956) is computed as:

$$LI = T_{500} - T_{P,500*} \tag{2}$$

where $T_{P,500*}$ is computed similarly to $T_{P,500}$, but the parcel is defined as having mean temperature (from the original sounding or a modified sounding using the predicted maximum temperature) and mean mixing ratio from the lowest 3000-foot layer. Since the lifting parcel has been defined several ways (see discussion in Craven *et al*., 2002), we considered the parcel as assuming mean thermal and moisture characteristics of the lowest 100 hPa, and lifted from layer's midpoint. The LI was originally utilized in the forecasting of severe thunderstorms and tornadoes in the U.S. (Peppler, 1988). Negative values are associated with unstable conditions, for example, $LI \leq -6^{o}C$ indicates very unstable conditions and strong potential for thunderstorms development. LI, in general, is lower than SWI.

3.3 K-Index (KI)

The KI (George, 1960) is defined as:

$$KI = (T_{850} - T_{500}) + T_{d,850} - (T_{700} - T_{d,700}) \tag{3}$$

The KI was developed for applications in the U.S. related to the occurrence of non-severe convective showers and thunderstorms (Peppler and Lamb, 1989). The likelihood of showers and thunderstorms increases for higher values of KI. $KI \geq +20^{o}C$ is related to increasing potential for occurrence of air mass thunderstorms. $KI > +40^{o}C$ indicates an extremely high probability of occurrence.

3.4 Total Totals Index (TT)

The TT (Miller, 1967) is calculated as:

$$TT = T_{d,850} - T_{500} + T_{850} - T_{500} \tag{4}$$

The TT was conceived to identify areas potentially favorable for severe weather occurrence in the U.S. (Peppler, 1988). The likelihood of severe development increases for higher values of TT. $TT \geq +44^{o}C$ is the suggested threshold over U.S. (Peppler and Lamb, 1989). $TT \geq +56^{o}C$ is associated with very unstable environments conducive to the development of numerous thunderstorms (including severe thunderstorms and scattered tornadoes).

3.5 Galvez-Davison Index (GDI)

The GDI [dimensionless] was designed for applications in the tropics and subtropics (including southeastern U.S.), and it is defined as (Galvez and Davison, 2014):

$$GDI = ECI + MWI + II (+ OC) \tag{5}$$

where:

- ▪ ECI corresponds to the equivalent potential temperature proxy (EPTP) core index intended to evaluate the convective instability of the mid-troposphere through the equivalent potential temperature (EPT) vertical profile.

- ▪ MWI corresponds to the mid-level warming index, which takes into consideration the effects of mid-levels troughs (cold air enhancing instability) and ridges (warm air enhancing stability).

- II is the inversion index designed to consider the existence of temperature inversions and dry air entrainment (conditions unfavorable for convection).

- OC is an optional correction recommended for the visualization of GDI over elevated mountain ranges when a gridded tool (e.g., Wingridds) is used for plotting this index.

The computation of GDI requires temperature and mixing ratio data at 950, 850, 700 and 500 hPa (and surface pressure for the OC), and it is fully described at http://www.wpc.ncep.noaa.gov/international/gdi/GDI_Calculation_Algorithm_20140314. pdf. Increasing GDI values indicate higher potential for thunderstorms development. For instance, GDI between 35 and 45 indicates the existence of potential for scattered thunderstorms and/or widespread shallow convection. GDI > 45 signals high potential for scattered to widespread thunderstorms (the reader can refer to http://www.wpc.ncep.noaa.gov/international/gdi/ for the complete interpretation of GDI values and further details on GDI).

Chapter 4. Data and Methodology

The methodology presented in this work considered comparisons between RAOBs with the closest NUCAPS retrievals and ECMWF analysis profiles collocated within a maximum radius of 50 km and ±1-hr time difference. It means that for each RAOB, SIPs were calculated (and compared) only if both NUCAPS and ECMWF profiles simultaneously match the previous criteria.

RAOBs, ECMWF and NUCAPS profiles were obtained from the NOAA Products Validation System (NPROVS), operated at the NOAA/NESDIS Center for Satellite Applications and Research (Reale *et al*., 2012). On a daily basis, and for a global coverage, NPROVS receives and processes atmospheric sounding products from multiple satellites, operational radiosonde and dropsonde observations, dedicated/reference RAOBs, and numerical weather prediction (NWP) outputs (e.g., ECMWF analyses and GFS 6-h forecasts), among other sources of data. The robust data processing, which includes quality control procedures and screening tests of the RAOBs, provides standardized criteria for the collocation and intercomparison of all datasets received. As a general strategy, any single sounding from each satellite system that is closest in space and time within a window of ±6 h and 250 km is collocated for each RAOB. However, NPROVS allows users to obtain collocated datasets with more strict time and spatial thresholds.

RAOBs used in this study are from two categories: (1) conventional radiosondes launched by the World Meteorological Organization upper air stations to support operational weather forecasting; and (2) satellite synchronized dedicated and reference

radiosondes, characterized by their optimum accuracy and well-known error characteristic (Nalli *et al*., 2013). The JPSS Calibration/Validation (Cal/Val) program and collaborating institutions have performed launches of dedicated RAOBs at several sites including the Atmospheric Radiation Measurement (ARM) Climate Research Facility, and the Pacific Missile Range Facility (PMRF); and over open-ocean by means of series of intensive AERosols and Ocean Science Expeditions (AEROSE) field experiments (Nalli *et al*., 2011). Reference RAOBs are from the Global Climate Observing System (GCOS) Reference Upper Air Network (GRUAN). Dedicated and reference RAOBs consist typically of RS92-SGP launched to coincide with satellite overpasses, usually between 15 to 60 min in advance to allow for balloon ascent through the lower troposphere (Nalli *et al*., 2013). Given that dedicated and reference RAOBs are not typically assimilated into NWP models, such measurements represent independent and high-quality references for purposes of satellite validation. However, their use is constrained by small sample sizes. For this reason, in this work, only mid-latitudes soundings could be utilized. An overview of the aforementioned concepts of RAOBs is given in Nalli *et al*. (2013).

The ECMWF analysis fields have a grid resolution of 0.25^{o} latitude $\times$ 0.25^{o} longitude with temperature and mixing ratio values at 91 sigma levels. (Details regarding the ECMWF model can be found online at http://www.ecmwf.int/en/forecasts/documentation-and-support).

Given that the NUCAPS AVTP and AVMP products are produced for fixed 100 pressure levels, the removal of those levels below the surface level was made by

31

comparisons with the GFS surface pressure (ancillary information required for the NUCAPS processing, as described in Chapter 2).

The evaluation was conducted separately over two latitudinal bands: mid-latitudes (60N to 30N) and tropics (30N to 30S). Over mid-latitudes, collocations with conventional RAOBs occurring from April 1st to September 30th of 2015 were considered, in order to focus on the warm season. In the case of dedicated/reference RAOBs, collocations were taken from the warm seasons of the years between 2013 and 2015. For the evaluation over the tropics, based on conventional RAOBs, the collocation matchups were created for the period December 2014 to December 2015. This approach ensured a very large sample of RAOBs producing approximately 9700 of conventional RAOBs and 300 dedicated RAOBs for mid-latitudes, and a sample of about 3700 conventional RAOBs for the tropic regions).

As shown in Chapter 3, most SIPs require temperature/moisture content information at specific pressure levels, such as 500, 700, 850, and 950 hPa. Since atmospheric parameters at these specific levels are not provided by the NUCAPS AVTPs/AVMPs products, a linear interpolation scheme was applied. The same interpolation scheme was employed to obtain moisture information at the surface level. The NUCAPS retrieval product Skin Temperature provided the information of temperature at the surface level.

Considering that NUCAPS AVMPs are vertical profiles of mixing ratio (in g/g), the conversion to dewpoint temperature follows the procedures described in Bolton (1980). The code devised for the computation of the LI is based on the work presented in

Doswell *et al*. (1982). The documentation for the calculation of Galvez-Davison index (GDI) is available online on the Weather Prediction Center/NCEP web page (http://www.wpc.ncep.noaa.gov/international/gdi/GDI_Calculation_Algorithm_20140314.pdf).

Chapter 5. Assessment of NUCAPS Temperature and Water Vapor Profiles

This chapter presents a general evaluation of the retrieved AVTPs and AVMPs generated by NUCAPS with respect to the reference RAOBs. ECMWF-derived profiles are also included to provide additional basis for comparison purposes. This preliminary evaluation is important since these profiles constitute the input data for computation of the air stability parameters presented in the subsequent chapter. For this reason, the analyses are mainly focused on levels of particular interest for such computation.

Before proceeding, it is important to provide some background on the validation metrics shown in the figures of this chapter. The thermodynamic profiles presented in this section were obtained from the NPROVS. In this system, the computation of validation statistics of a retrieved profile (also valid for numeric model outputs) relative to RAOBs, follows the methodology presented in Nalli *et al*. (2013). The initial procedure of the method requires the reduction of the high-resolution RAOB profile to a lower vertical resolution. In this work, 100 layers were used as the basis for the computation of validation statistics for the temperature and water vapor profiles. The definitions of the error metrics are briefly presented below, noticing that fundamental differences exist for the assessment of temperature and water vapor profiles.

For AVTPs, metrics are calculated for the temperature difference, at a matchup location j, between the retrieved temperature (denoted with a hat) and the reference temperature (from RAOBs), defined as:

$$\Delta T_{\mathcal{L},j} \equiv \widehat{T}_{\mathcal{L},j} - T_{\mathcal{L},j}, \qquad \mathcal{L} = 1, 2, \ldots, m \tag{6}$$

where $\mathcal{L}$ represents the layer being evaluated (m is the number of layers). Given equation (6), the bias statistics (BIAS), a measure of central tendency, is the mean difference computed via eq. (7):

$$BIAS(\Delta T_{\mathcal{L}}) \equiv \overline{\Delta T_{\mathcal{L}}} = \frac{1}{n_j} \sum_{j=1}^{n_j} \Delta T_{\mathcal{L},j} \tag{7}$$

where n_j refers to the matchup sample size. The standard deviation (STD), used to express the variability around the mean, is computed as:

$$STD(\Delta T_{\mathcal{L}}) = \sqrt{[RMS(\Delta T_{\mathcal{L}})]^2 - [BIAS(\Delta T_{\mathcal{L}})]^2} \tag{8}$$

where $RMS(\Delta T_{\mathcal{L}})$ is the root-mean-square temperature difference given by:

$$RMS(\Delta T_{\mathcal{L}}) = \sqrt{\frac{1}{n_j} \sum_{j=1}^{n_j} (\Delta T_{\mathcal{L},j})^2} \tag{9}$$

For the computation of the metrics needed to evaluate the AVMPs performance, it is necessary to take into account the great variability of water vapor in the entire atmosphere. From layer mass abundances, $q_{\mathcal{L}}$ (in g/cm^2), the fractional deviation, at a matchup location j, is calculated based upon the difference between the retrieved and the reference value:

$$\Delta q_{\mathcal{L},j} \equiv \frac{\hat{q}_{\mathcal{L},j} - q_{\mathcal{L},j}}{q_{\mathcal{L},j}} , \qquad \mathcal{L} = 1, 2, \dots, m \tag{10}$$

In theory, the RMS, BIAS and STD statistics could be obtained by replacing $\Delta T_{\mathcal{L}}$ by $\Delta q_{\mathcal{L}}$ in equations (7), (8) and (9). However, as pointed out by Nalli *et al*. (2013), the

denominator in (10) can lead to a large $\Delta q_{\mathcal{L},j}$ in dry atmospheres (upper troposphere or polar regions), skewing the statistics toward these cases. To minimize this situation, weighted means were devised and the proper definitions are as follows:

$$BIAS(\Delta q_{\mathcal{L}}) = \frac{\sum_{j=1}^{n_j} W_{\mathcal{L},j} \Delta q_{\mathcal{L},j}}{\sum_{j=1}^{n_j} W_{\mathcal{L},j}} \tag{11}$$

$$STD(\Delta q_{\mathcal{L}}) = \sqrt{[RMS(\Delta q_{\mathcal{L}})]^2 - [BIAS(\Delta q_{\mathcal{L}})]^2} \tag{12}$$

where $RMS(\Delta q_{\mathcal{L}})$ is given by:

$$RMS(\Delta q_{\mathcal{L}}) = \sqrt{\frac{\sum_{j=1}^{n_j} W_{\mathcal{L},j} (\Delta q_{\mathcal{L},j})^2}{\sum_{j=1}^{n_j} W_{\mathcal{L},j}}} \tag{13}$$

The water vapor weighting factor, $W_{\mathcal{L},j}$, is defined as:

$$W_{\mathcal{L},j} \equiv (\Delta q_{\mathcal{L}})^2 = W^2 \tag{14}$$

Having defined the validation metrics, it is now possible to examine Figure 1, which shows the STD and BIAS statistics calculated from the temperature differences between NUCAPS (or ECMWF) profiles and conventional RAOBs over mid-latitudes and tropics. In both cases, the ECMWF temperature profiles present the highest level of agreement with respect to the conventional RAOBs, as is clearly identified by the consistently lowest values of STD and BIAS observed at all levels. However, it is known that both datasets are not totally independent since conventional RAOBs have been long assimilated by the ECMWF data assimilation system (Simmons and Hollingsworth, 2002).
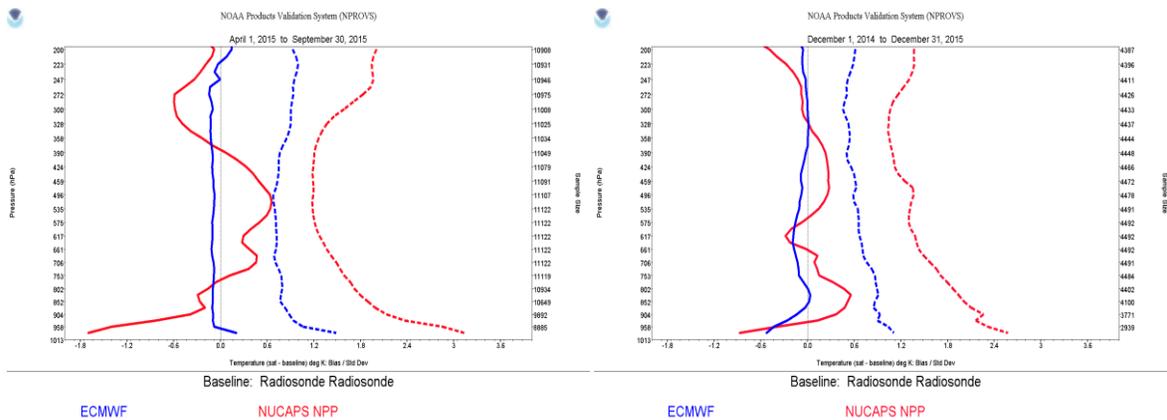
36

Figure 1. NPROVS-derived BIAS (solid line) and STD (dashed line) statistics of NUCAPS (red) and ECMWF (blue) relative to conventional RAOBs matchups - AVTP: (left) mid-latitudes and (right) tropics.

At mid-latitudes (Fig.1; left panel), it is noticeable that the skill of NUCAPS decreases downward, showing the lowest performance near the surface, where BIAS and STD values are around -1.7K and 3.2K, respectively. The maximum negative BIAS near the surface indicates an underestimation of NUCAPS-retrieved temperatures at those levels (cold BIAS). On the other hand, the BIAS becomes slightly positive between 750 and 400 hPa, where maximum values of about 0.6K are observed, whereas the STD decreases over these particular pressure levels. The negative BIAS observed between 250 and 350 hPa, results from the inability of NUCAPS to resolve for the temperature structure over the tropopause.

Results over the tropical region (Fig.1; right panel) show better skill of NUCAPS retrieved temperature over several pressure levels, particularly near surface. However, the observed tendency of NUCAPS to degrade as approaching the surface is also found. This performance is expected and is associated to the lower information content found in the CrIS/ATMS observations to sense the atmospheric temperature variations near the

37

surface. Quantitatively, the BIAS and STD magnitudes near surface are about -0.9K and 2.6K, respectively. At lower levels, both NUCAPS and ECMWF BIAS profiles are more similar in comparison to the mid-latitudes case, but NUCAPS exhibits a slight warm BIAS close to 0.5K. Like the mid-latitudes case, NUCAPS STD decreases toward the mid-level pressures, having a minimum value near 300 hPa.

In general, NUCAPS shows better bias performance over the tropics, while its capability to retrieve temperature is degraded near the surface, situation that is more pronounced over mid-latitudes. In the case of ECMWF, it is noteworthy the low bias observed over mid-latitudes, which is probably associated with the larger amount of observations assimilated over those regions, than over the tropics, explaining the better performance in terms of bias over mid-latitudes.

Figure 2 depicts the STD and BIAS of AVMPs derived from NUCAPS and ECMWF, expressed in terms of percent errors and obtained by multiplying equations (11) and (12) by 100.
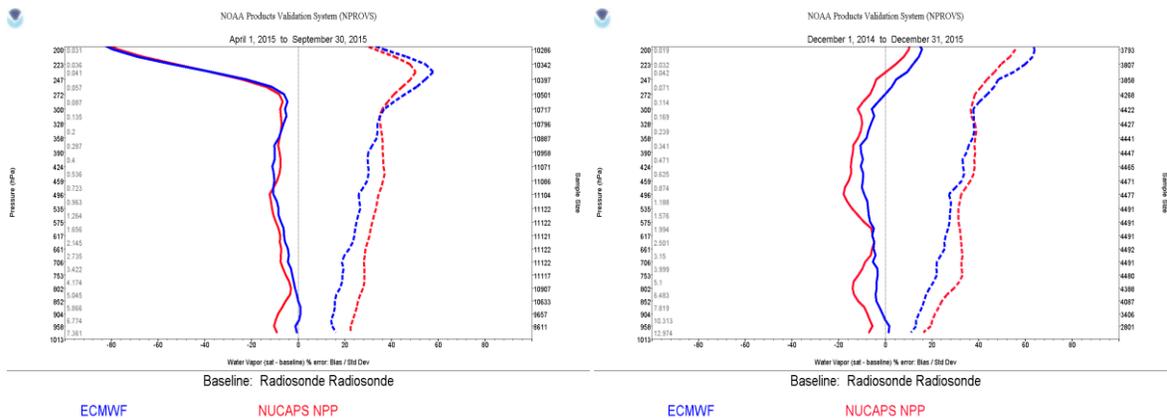

Figure 2. NPROVS-derived BIAS (solid line) and STD (dashed line) statistics of NUCAPS (red) and ECMWF (blue) relative to conventional RAOBs matchups - AVMP: (left) mid-latitudes and (right) tropics.

Unlike the AVTP case, the overall accuracy of the AVMP profiles does not show a rapid degradation as approaching the surface, showing bias values around 10%. At both regions, NUCAPS and ECMWF profiles exhibit distinct similarity throughout the atmosphere. In general, ECMWF statistics percent errors are smaller, but the overall performance of both AVMPs is comparable. Below 300 hPa, a slight negative (dry) BIAS is evident in both regions for each AVMP. In this case, the largest magnitudes of the BIAS computed for the NUCAPS AVMPs are found in the tropics, showing a bias of about 16% around 800 and 500 hPa.

It is important to highlight that the statistical performances presented in Figures 1 and 2, for NUCAPS and ECMWF, include (1) time and space collocation errors, (2) representativeness errors, and (3) intrinsic RAOBs errors. Since these errors can be systematic or random, their impact can be reflected in both the bias and standard deviation. In this respect, it is expected that the actual uncertainties of NUCAPS and ECMWF are smaller than the ones reported here.

Since most SIPs require information at specific pressure levels, such as 500, 700, 850, and 950 hPa, the assessment of the NUCAPS soundings performance at these particular levels is presented in Tables 3 to 6, showing the evaluation of NUCAPS (also including ECMWF) with respect to conventional RAOBs. Evaluations are based on the same metrics previously shown, along with the coefficient of determination (r^2). A basic interpretation of r^2 comes from the concept of simple linear regression analysis, in which the square root of r^2 is the linear (or Pearson) correlation coefficient (r) (Wilks, 2011). In this work, the r^2 parameter is used to understand the proportion of the variance shared by

the temperature and water vapor measured by the RAOBs and the corresponding ones derived from NUCAPS and ECMWF.

Table 3. Statistics over mid-latitudes computed at different pressure levels: AVTP.

Level (hPa)	STD (K)		BIAS (K)		r^2		Npts
	ECMWF	NUCAPS	ECMWF	NUCAPS	ECMWF	NUCAPS	
496.6	0.680	1.190	-0.077	0.636	0.988	0.956	11107
706.5	0.706	1.490	-0.090	0.460	0.989	0.949	11122
852.7	0.769	1.893	-0.100	-0.264	0.990	0.937	10649
958.5	1.060	2.855	-0.082	-1.399	0.978	0.805	8885

Table 4. Statistics over tropics computed at different pressure levels: AVTP.

Level (hPa)	STD (K)		BIAS (K)		r^2		Npts
	ECMWF	NUCAPS	ECMWF	NUCAPS	ECMWF	NUCAPS	
496.6	0.586	1.360	-0.081	0.256	0.980	0.893	4478
706.5	0.761	1.576	-0.129	0.089	0.972	0.882	4491
852.7	0.863	2.009	0.021	0.517	0.982	0.898	4100
958.5	1.036	2.315	-0.435	-0.389	0.961	0.831	2939

In agreement with the mid-latitude analysis shown in Figure 1 (left panel), Table 3 reveals that the temperature at 958.5 hPa presents the highest value of STD, the largest magnitude of BIAS (cold BIAS) and the smallest r^2 for NUCAPS. Over the tropics (Table 4), a 1 K lower BIAS is found for the 958.5 hPa level, accompanied by a smaller STD (by about 0.5K) and a slight increase in r^2. At 852.7 hPa, NUCAPS exhibits a slight warm BIAS of close to 0.5K over the tropics, contrasting to a cold BIAS of approximately -0.3K at mid-latitudes. In addition, from Tables 3 and 4 it is found that the NUCAPS temperature STD is approximately two times larger than the one found for the ECMWF temperature for both the tropics and mid-latitudes.

From Tables 5 and 6, it can be observed that the STD of the NUCAPS water vapor is comparable over both regions, whereas the r^2 is higher over the tropics. On the other hand, the BIAS of NUCAPS shows slightly lower values over mid-latitudes, for practically all pressure levels.

Table 5. Statistics over mid-latitudes computed at different pressure levels: AVMP.

Level (hPa)	STD (%)		BIAS (%)		r^2		Npts
	ECMWF	NUCAPS	ECMWF	NUCAPS	ECMWF	NUCAPS	
496.6	25.815	34.365	-10.568	-12.155	0.808	0.672	11104
706.5	18.666	28.013	-4.459	-7.509	0.860	0.672	11122
852.7	15.647	25.633	-0.037	-5.247	0.847	0.556	10633
958.5	14.470	22.489	-1.147	-10.381	0.857	0.587	8611

Table 6. Statistics over tropics computed at different pressure levels: AVMP.

Level (hPa)	STD (%)		BIAS (%)		r^2		Npts
	ECMWF	NUCAPS	ECMWF	NUCAPS	ECMWF	NUCAPS	
496.6	27.249	32.551	-8.962	-17.834	0.846	0.746	4477
706.5	22.107	32.670	-5.281	-8.576	0.855	0.682	4491
852.7	16.507	24.231	-3.834	-11.714	0.879	0.710	4087
958.5	13.158	19.590	1.785	-5.533	0.900	0.759	2801

As discussed in Chapter 6, all previous results and analyses play a key role when interpreting the statistical results derived from the evaluation of NUCAPS derived SIPs.

Chapter 6. Results

This chapter is dedicated to the evaluation of the NUCAPS-derived SIPs. Over the tropics, only the TPW, KI and GDI are evaluated since, by definition or by traditional use (e.g., KI), these parameters are considered useful for operational forecasting applications over this region. Relevant assumptions and considerations carried out in this validation are: (1) The STD and BIAS are calculated by computing the difference between the values of the SIPs derived from NUCAPS or ECMWF and the RAOBs SIP values; and (2) for comparison purposes, a least squares procedure was used to calculate the best-fit curve, assuming a 2nd degree polynomial of the form $y = a_0 + a_1x + a_2x^2$, between the pairs RAOBs and NUCAPS SIPs and RAOBs and ECMWF SIPs. In addition, the statistical results presented in this chapter include errors due to collocation carried-out over time and space, errors associated with representativeness of the observed atmosphere (NUCAPS volume-averaged vs. RAOB point observations), as well as intrinsic errors found in the RAOB instrumentation. All these errors should be accounted when evaluating the presented statistical performance of the derived SIPs, since those errors contribute to increase the actual errors. Due to that, the actual performance of the NUCAPS-derived SIPs is expected to be higher than the results presented in this chapter.

The results presented in this chapter will be divided in two major sections. One that corresponds to the large sample of conventional RAOBs, and another where dedicated/reference radiosondes were used. The latter is expected to reduce the satellite-RAOBs collocation errors due to its high synchronization with the satellite observations (typically 15-60 minutes of time difference) and the errors associated with the radiosonde

observations, due to the high accuracy and quality of the radiosonde sensors. As previously mentioned, a disadvantage of dedicated/reference radiosondes basically relies on the small sample size as compared to the robust sample size of the conventional RAOBs.

6.1 Conventional Radiosondes

6.1.1 TPW

The NUCAPS and RAOB versions of TPW show high level of statistical agreement (Fig. 3), especially over the tropics, where remarkable values of r^2 (above 0.85) are observed. Both scatter plots presented in Figure 3 show that the a_2 and a_1 coefficients are very close to zero, and one, respectively, indicating a very strong linear relationship between the pairs of SIPs under evaluation. It is found that the NUCAPS BIAS is around -2 mm over both regions, implying a slight underestimation of TPW values. This is shown graphically by the scatter diagrams in Figure 3 (top and bottom; left), in which most NUCAPS TPW points are below the reference "perfect-fit" line (in black), particularly for values of TPW above 15 mm. This pattern is also evident on the bar histograms, where NUCAPS frequencies are somewhat below RAOBs as well as ECMWF for the categories corresponding to high TPW values above 25 mm over mid-latitudes, and above 40 mm over the tropics.

The fact that NUCAPS TPW values agree closely with conventional RAOBs counterparts over both areas, indicates that NUCAPS is able to generate a high-quality TPW product, containing meaningful information about the integrated amount of atmospheric water vapor. Due to the high agreement found over a wide range of observed

43

TPW values, going from a few mm to large amounts, the NUCAPS TPW is well suited to be employed in the forecasting process, which is of significant importance given that TPW is a widely used parameter to assess the potential for heavy precipitation at a location (typically associated with plumes of elevated TPW values). However, forecasters should be mindful of the fact that NUCAPS TPW magnitudes will tend to be lower than their equivalent RAOBs versions, particularly for very high values of TPW.
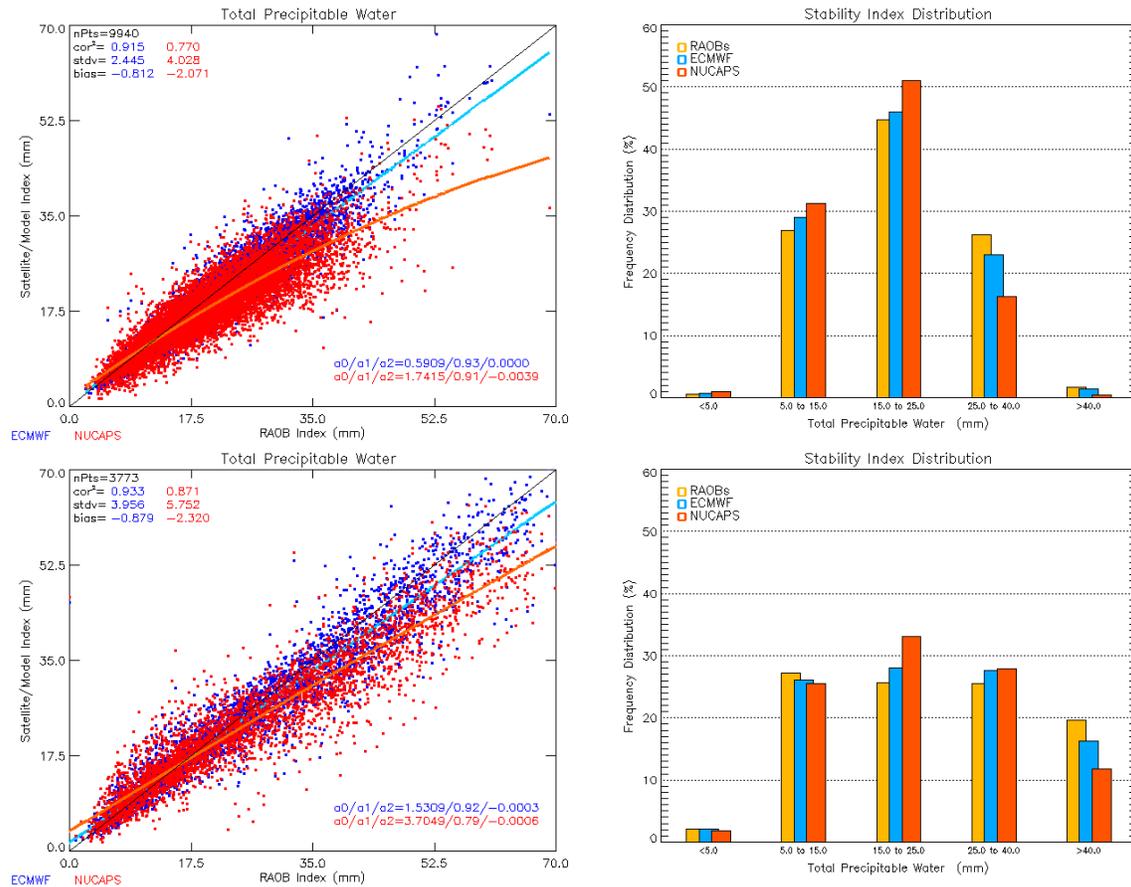

Figure 3. Scatter plots of conventional RAOBs versus NUCAPS/ECMWF TPW for: (top left) mid-latitudes and (bottom left) tropics. Histograms of RAOBs/ECMWF/NUCAPS TPW for: (top right) mid-latitudes and (bottom right) tropics.

6.1.2 SWI and LI

Due to the conceptual similarities between the SWI and LI, results derived from those indices are summarized in this section. The scatter plots presented in Figure 4 (top and bottom; left) indicate that, in general, NUCAPS exhibits intermediate levels of agreement with respect to RAOB SIPs, showing an r^2 of 0.403 (r=0.63) and 0.480 (r=0.69) for the LI and SWI, respectively. In the case of the STD, results show a value of 3.1°C for the SWI, and 3.9°C for the LI, revealing considerable variability of the SWI and LI values derived by NUCAPS with respect to the corresponding indices computed from RAOBs. As the RAOBs SWI and LI values approach to zero, their NUCAPS counterparts tend to have larger magnitudes (note that most NUCAPS points are above the reference "perfect-fit" line in this case). This pattern can also be visualized on the histograms (Fig. 4), where the frequency of the NUCAPS derived indices is consistently lower with respect to the RAOB and ECMWF computed indices for values below 3.0°C. Given that small SWI and LI values are associated with high instability, previous results suggest that NUCAPS derived SWI and LI exhibit certain tendency for underestimation of the unstable atmospheric conditions. This is of special relevance given that the LI is among the most commonly used stability products on the operational forecasting routine.
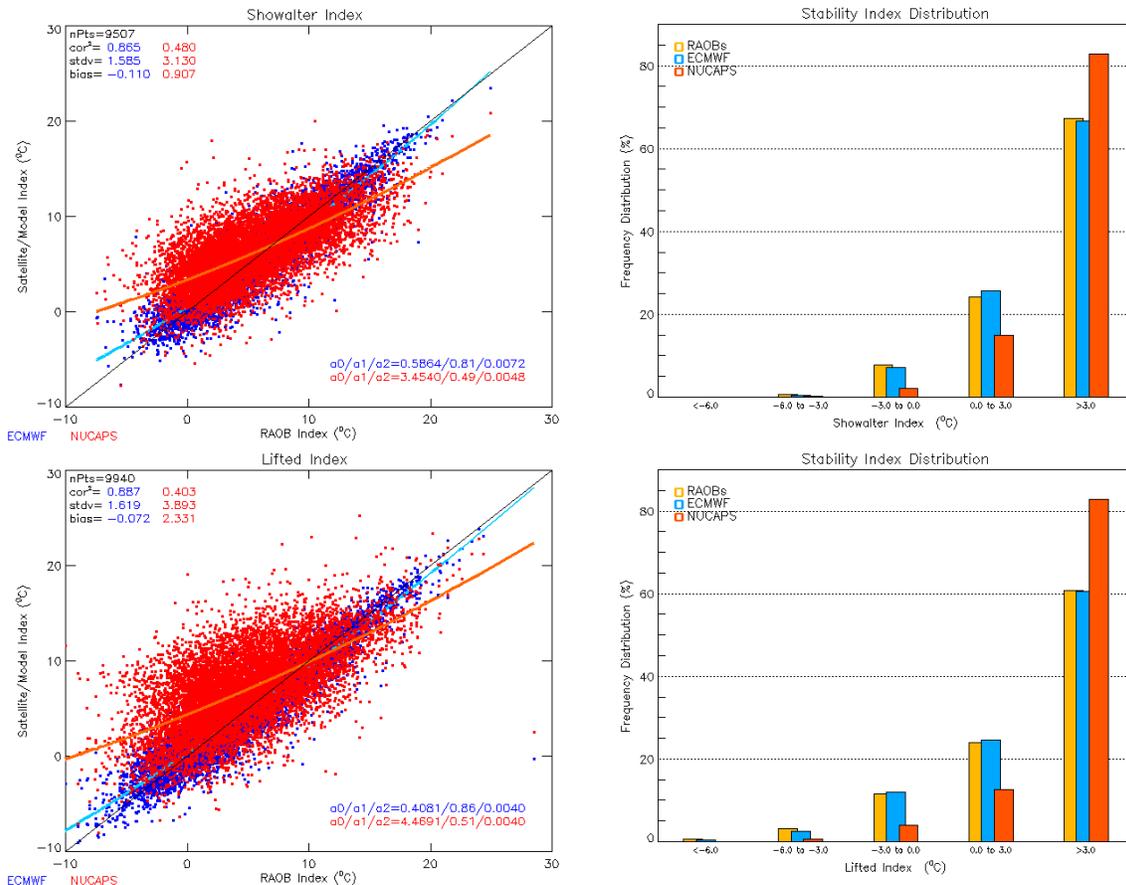
Figure 4. Scatter plots of conventional RAOBs versus NUCAPS/ECMWF versions of SWI (top left) and LI (bottom left) for mid-latitudes. Histograms of RAOBs/ECMWF/NUCAPS SWI (top right) and LI (bottom right) for mid-latitudes.

By definition, the SWI and LI involve the lifting of low-level air parcels to the 500-hPa level, where parcels temperatures are compared with the ambient temperature at that level. An unsaturated air parcel undergoes a dry adiabatic ascent, but if it becomes saturated (the pressure level where saturation first occurs defines the LCL), its subsequent ascent will follow a pseudo adiabatic process. In this respect, the NUCAPS derived thermodynamic characteristics of the low-level parcel as well as the ambient temperature at 500-hPa are determinant to the quality of the resulting SWI and LI indices. As noted earlier, in the discussion presented in Chapter 5, the NUCAPS AVTPs are cold

46

biased (i.e., NUCAPS AVTPs tend to be on average lower than RAOBs temperatures) at the lowest levels and slightly warm biased in the middle troposphere at mid-latitudes (see Fig. 1; left and Table 3). Moreover, NUCAPS AVMPs are slightly dry biased below 300 hPa (see Fig. 2; left and Table 5). Considering the thermodynamics theory of the lifting process, and assuming dewpoint depressions that allow low-level air parcels reach saturation, with the water vapor content (i.e., dewpoint) held constant, colder low-level air parcels in adiabatic ascent result in lower 500-hPa parcel temperatures. With the temperature held constant, drier low-level air parcels in adiabatic ascent also result in lower 500-hPa parcel temperatures due to the reduced contribution of the latent heating. As part of the LI computation, temperature and mixing ratio from atmospheric levels within the lowest 100 hPa were averaged to define the mean parcel (MP) characteristics. In this case, the systematic errors (cold and dry biases) of the NUCAPS thermodynamics profiles at the lower levels are responsible for generating 500-hPa parcel temperatures colder than those produced by RAOBs. Mathematically speaking, these factors tend to reduce the value of the second term of eq. (2). In addition, the 500-hPa NUCAPS warm BIAS of around 0.6K (see Table 3) signifies that the NUCAPS-derived 500-hPa ambient temperatures tend to be slightly higher than the corresponding RAOBs-derived temperatures, which contributes to increase the values of the first term of eq. (1). Thus, NUCAPS tends to produce less buoyant parcels, which leads to more positive (or less negative) LIs, as observed in the Figure 4 (bottom; left). Similar considerations apply for the interpretation of the results of NUCAPS SWI. In this case, the NUCAPS derived SWI shows better agreement with respect to the RAOBs values because the hypothetical

47

parcel assumes thermal and moisture characteristics of the 850-hPa level. For this specific level, the NUCAPS temperature and moisture biases are low (about -0.26 K for temperature and -5.25% for water vapor, as shown in Tables 3 and 5, respectively), which introduces smaller errors into the NUCAPS SWI computation in comparison with the NUCAPS LI case. As a consequence, the NUCAPS SWI is superior to the NUCAPS LI in terms of agreement with conventional RAOBs, since the latter is more affected by the low-level biases of the NUCAPS AVTPs and AVMPs.

It should also be mentioned that due to the fact that satellites, in reality, provide volume-averaged information rather than point data, like the radiosondes, intrinsic differences are expected when comparing SIPs derived from satellite observations against SIPs produced from RAOBs. For example, over regions where large atmospheric inhomogeneities are observed within the satellite field-of-view, SIPs corresponding to an average of the observed atmosphere will be produced by NUCAPS. In contrast, radiosondes are expected to provide SIPs representative of the launch location. In this respect, it is important to highlight the presence of representativeness errors found in RAOBs associated with the drift experienced during the radiosonde ascending, which could reach several kilometers. Since satellites perform nearly instantaneous observations, they do not show this type of representativeness error. These intrinsic differences clearly contribute to increase the differences found during the NUCAPS and RAOBs comparisons.

The fact that the parcel mean temperature at the lowest 100 hPa and the parcel mean dewpoint temperature at the lowest 100 hPa are indispensable input parameters for

the computation of LI motivates a specific analysis of the ability of NUCAPS in deriving the MP characteristics. These results are presented in Figure 5.
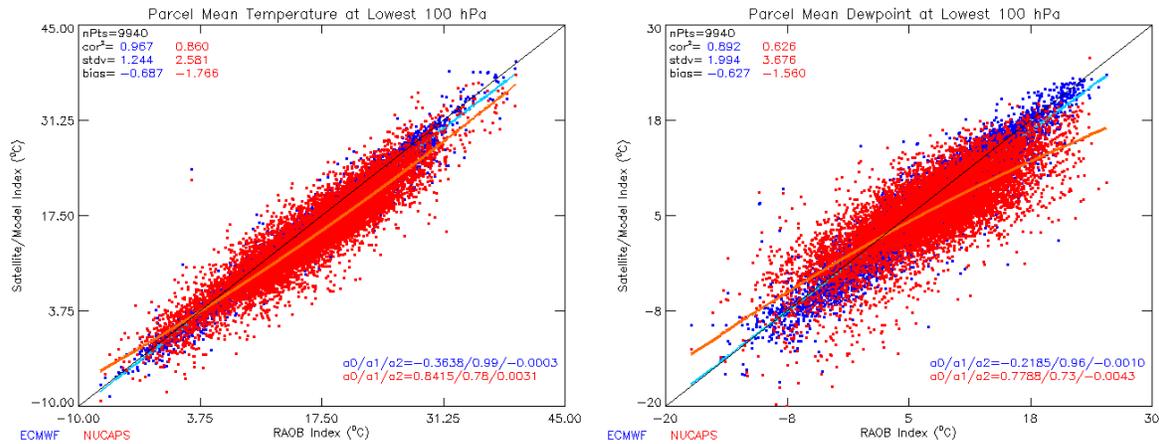

Figure 5. Scatter plots of conventional RAOBs versus NUCAPS/ECMWF versions of Parcel Mean Temperature at Lowest 100 hPa (left) and Parcel Mean Dewpoint at Lowest 100 hPa (right) for mid-latitudes.

In agreement with the discussion about the quality of NUCAPS temperature and water vapor presented in Chapter 5, the NUCAPS-derived MPs tend to be colder and drier than the RAOBs-derived versions. Figure 5 (left panel) reveals high level of agreement of NUCAPS in relation to RAOBs as can be observed by the high r^2. However, it is possible to observe a negative BIAS in the NUCAPS estimation. This result is consistent and in line with the negative BIAS already observed in Figure 1, when evaluating the quality of the NUCAPS retrieved temperature. For the NUCAPS parcel mean dewpoint at the lowest 100 hPa (Fig. 5; right panel), calculated from the average of NUCAPS mixing ratio data from all available levels within 100 hPa of the surface, the r^2 decreases to about 0.6, but it is still quite high. The negative BIAS observed here, which is about twice the one observed for the ECMWF case, is the result of the negative biases found in the NUCAPS water vapor near the surface, as shown in Figure 2, for mid-latitudes. Furthermore, the NUCAPS STD is larger for dewpoints than for temperatures.

49

In this respect, NUCAPS STD is near 3.7^{o}C for dewpoint, which is almost two times the corresponding ECMWF STD of about 2.0^{o}C. Those results show that NUCAPS temperature is in better agreement with respect to RAOBs over the 100 hPa layer closest to the surface, than water vapor, which is expected due to the lower information content found in the radiometric observations to retrieve moisture as compared to temperature near the surface.

Since the calculation of LI is the most complex among all parameters in the current study, it is possible to infer that the statistics of this index are the most affected by the intrinsic differences between the AVTPs/AVMPs derived by NUCAPS and RAOBs. Such differences are inevitably amplified by the various steps of the computation, resulting in a cumulative effect on the final verification metrics.

6.1.3 KI

Figure 6 presents the evaluation of the KI, traditionally used for the short-term forecasting of non-severe thunderstorms. The scatter plots show that the NUCAPS KI compares relatively well with respect to the RAOBs-derived values, with similar performance over the tropics and mid-latitudes. Values of r^2 around 0.6 and BIAS magnitudes of about 1°C are found when comparing KI values estimated from NUCAPS and RAOBs. With respect to the STD, both ECMWF and NUCAPS show larger values over the tropics than over mid-latitudes. From Table 3 and Table 4, as well as from the KI definition (see Chapter 3), it is possible to identify that the larger STD observed over the tropics by ECMWF and NUCAPS can be explained by the larger values of tropics temperature STD found at 700 and 850, as well as at 500 hPa, particularly for NUCAPS.

Furthermore, from Figure 6, it is possible to identify that the STD for the NUCAPS KI is approximately 1.5 times the STD found for ECMWF. This value compares and agrees with the magnitude of the temperature STD reported in Tables 3 and 4 (and discussed in Chapter 5). Those observations clearly show the impact of the quality of the NUCAPS AVTP in the computation of the KI.
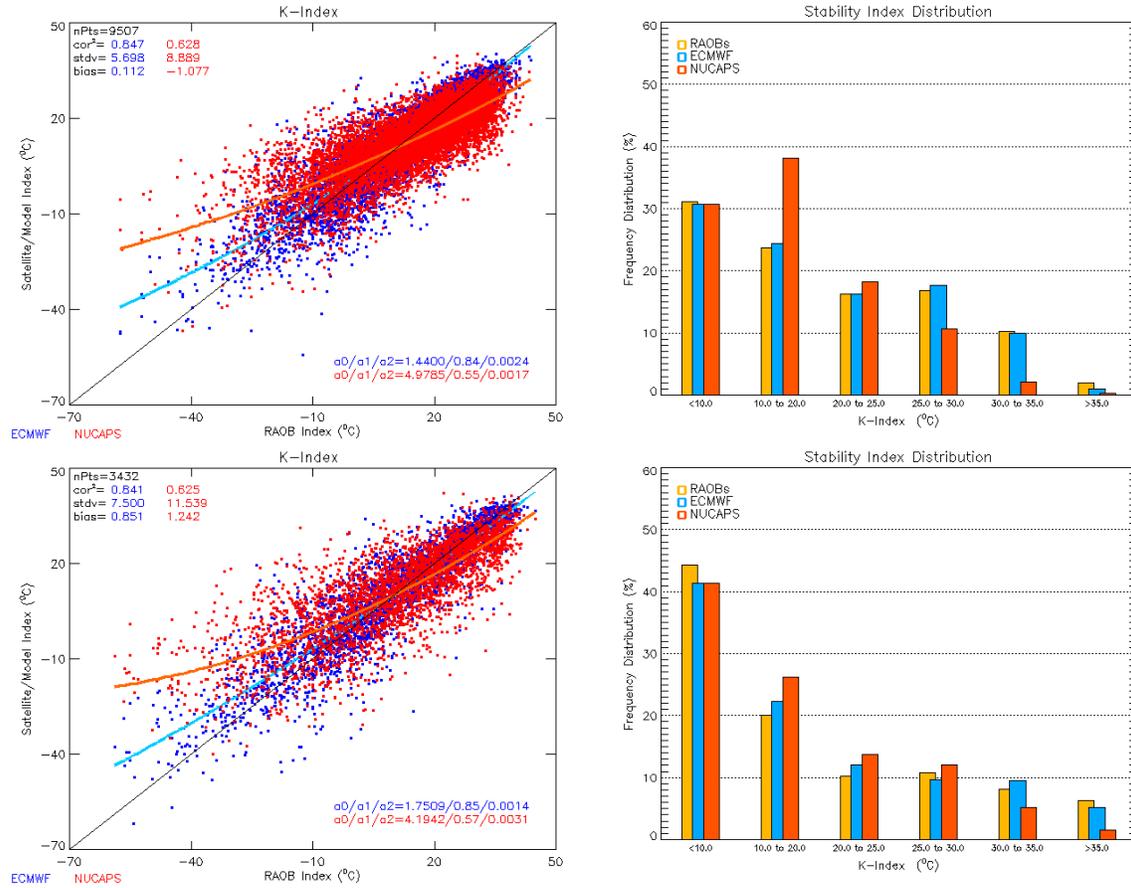

Figure 6. Scatter plots of conventional RAOBs versus NUCAPS/ECMWF KI for: (top left) mid-latitudes and (bottom left) tropics. Histograms of RAOBs/ECMWF/NUCAPS KI for: (top right) mid-latitudes and (bottom right) tropics.

Histograms of Figure 6 show that NUCAPS KI poses similar pattern of frequency distribution as compared to RAOB and ECMWF, except over the 10-20°C interval, where NUCAPS tends to estimate more KI cases, particularly over mid-latitudes.

51

The scatter plots also show how NUCAPS tends to underestimate the KI above approximately 10°C. By using the fitted coefficients of the NUCAPS best-fit curve, mid-latitudes (tropics) NUCAPS KI values are about 3 (3), 7 (6) and 9 (7) ^{o}C below RAOBs KI values of 20, 30 and 35°C, respectively. A consequence of that is the consistent decrease in the frequency of the NUCAPS KI values above 30°C, over the tropics, and above 25°C, over mid-latitudes, as shown by the histograms.

The scatter plots show that the RAOBs/NUCAPS differences are larger for the very stable RAOBs-defined values below -10°C. From the perspective of the forecaster using the NUCAPS KI product, all values below 10°C fall within the same category of very stable atmospheric conditions, which do not require closely monitoring. These situations are, in general, well resolved by NUCAPS, as shown by the histograms of Figure 6, in which the percent frequencies of NUCAPS KI cases below 10°C are similar to the ECMWF and RAOBs.

In summary, current results indicate that NUCAPS and RAOBs KI values are highly correlated, which encourage operational applications of the NUCAPS KI. As seen above, NUCAPS KI is able to identify very stable conditions (defined by RAOBs KI below 10°C), despite showing values that do not closely agree with RAOBs values. However, in this type of situation, forecasters are more interested in the correct classification of a stable case than in the exact value of the index. For more unstable conditions with RAOBs-defined KI values above 10°C, in special, situations with higher likelihood of thunderstorms onset (RAOBs KI above 30°C), forecasters should take into account the fact that NUCAPS KI tends to be an underestimate of the RAOBs value.

6.1.4 TT

Figure 7 depicts the scatter plot, the statistical scores and the histogram for the TT evaluation. Results show that TT exhibits an intermediate level of agreement with r^2 of 0.475 corresponding to an r of about 0.69. There is a low BIAS of -1.261^{o}C and a moderate STD of about 5.7^{o}C, which is approximately two times larger than the ECMWF STD. The latter is in line with the fact that the magnitude of the NUCAPS temperature STD at 850 and 500 hPa, as well as the water vapor STD at 850 hPa are about two times larger than the ECMWF corresponding STDs (see TT definition and Tables 3 and 5).
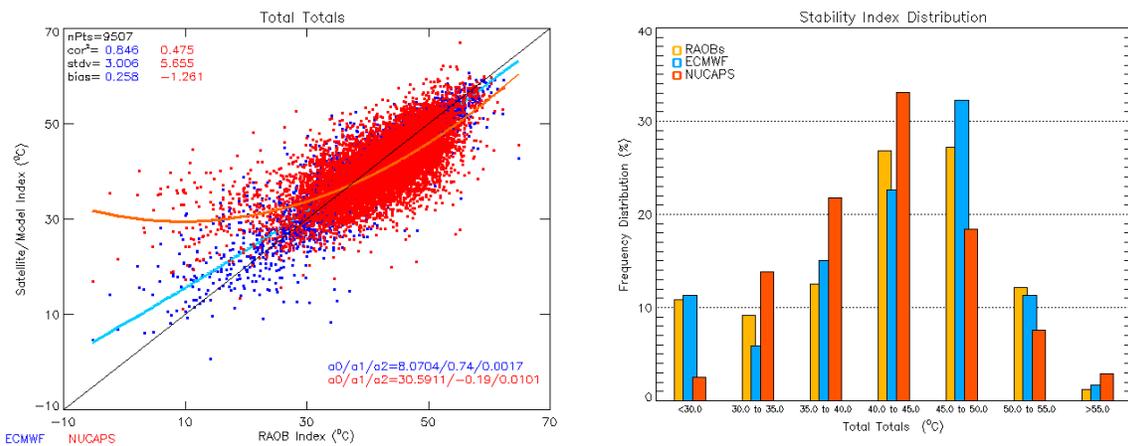

Figure 7. Scatter plot of conventional RAOBs versus NUCAPS/ECMWF versions of TT (left) for mid-latitudes. Histogram of RAOBs/ECMWF/NUCAPS TT (right) for mid-latitudes.

The negative BIAS indicates an overall NUCAPS tendency for underestimation of the RAOBs TT values. However, from the histogram (Fig. 7; right panel), it can be noted that this tendency is mainly driven by the NUCAPS TT values between 45 and 55°C. From the NUCAPS best-fit curve, NUCAPS TT values of about 3, 4 and 5°C below RAOBs TT values of 45, 50 and 55°C, respectively, can be expected. In comparison with RAOBs and ECMWF, there are fewer cases of NUCAPS TT points below 30°C. This is due to the fact that part of the RAOBs TT points of 30°C or less corresponds to higher

NUCAPS values, mainly between 30 to 40°C, as shown by the scatter plot. It is clear that the category of the lowest RAOBs-defined TT values (associated with very stable atmospheric conditions), in special below 20°C, contains large RAOBs/NUCAPS discrepancies that are negatively influencing the statistics in spite of the few cases.

6.1.5 GDI

The scatter plot (Fig. 8) shows r^2 of 0.603 (r about 0.78) when NUCAPS GDI is compared against the corresponding RAOBs values. This means that NUCAPS GDI accounts for approximately 60% of the variance of RAOBs GDI, although with a relatively high STD of 12.
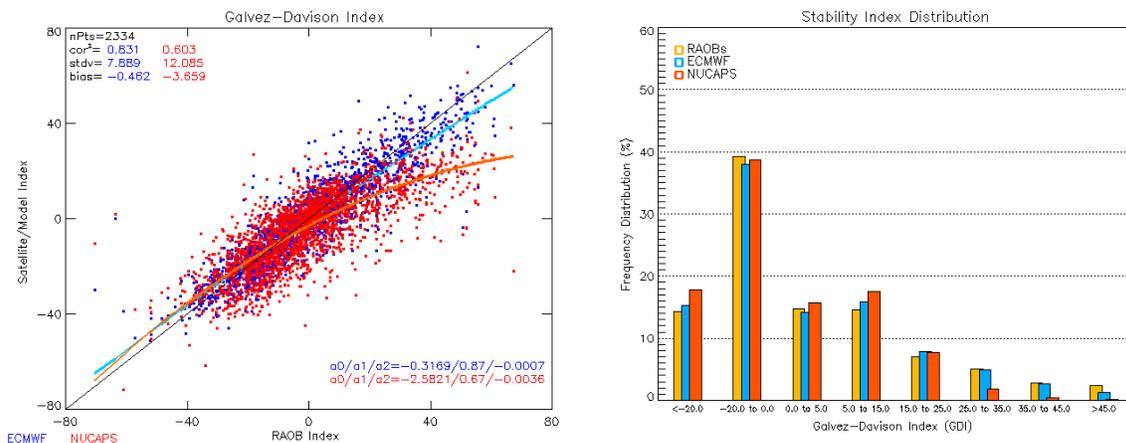

Figure 8. Scatter plot of conventional RAOBs versus NUCAPS/ECMWF versions of GDI (left) for tropics. Histogram of RAOBs/ECMWF/NUCAPS GDI (right) for tropics.

The negative BIAS indicates that NUCAPS GDI in general underestimates RAOBs GDI, particularly for RAOBs GDI values above 10. This is especially true for the highest GDI values, where NUCAPS GDI potential for resolving the most intense cases of tropical convective instability (GDI > 35) seems somewhat restricted. For example, for

54

RAOBs GDI values near 10, NUCAPS GDI estimates values close to 4. However, for RAOBs GDI values in the vicinity of 35, NUCAPS estimates GDI values around 16.

The GDI is calculated with temperatures and mixing ratios at 950, 850, 700 and 500 hPa. The thermodynamic properties at those levels are used during several stages of the multi-step calculation of GDI (see Chapter 3). Thus, it is reasonable to suggest that there is a cumulative effect generated by the RAOBs/NUCAPS differences in temperature and water vapor affecting the agreement between the NUCAPS and RAOBs versions of GDI.

More specifically, the calculation of GDI is highly dependent on the equivalent potential temperature (EPT), an important thermodynamic parameter that incorporates both temperature and moisture content (mixing ratio) on its formulation (highly accurate formulas for EPT are given by Davies-Jones, 2009). The EPT is defined as the temperature an air parcel would have if lifted dry adiabatically to its LCL, and then pseudo adiabatically (with respect to water saturation) to zero pressure, condensing all its water vapor, dropping out condensed water, and finally brought down dry adiabatically to 1000 hPa (Bolton, 1980; Bryan, 2008). Conceptually, the variation of EPT with height is a criterion to assess the convective (or potential) stability of the atmosphere (Wallace and Hobbs, 2006). Therefore, GDI requires the computation of EPT profiles to diagnose (1) warm moist unstable atmospheric conditions, and (2) subsidence (trade wind) inversions (localizing the decrease in the moisture content of a column associated with the temperature inversion). From Tables 4 and 6, the NUCAPS temperature BIAS ranges from -0.4 to 0.5K, whereas the NUCAPS water vapor BIAS ranges from -5 to -17%,

showing a consistent pattern of negative biases (i.e., NUCAPS AVMPs tend to be on average drier than RAOBs data). As a result of the dependence of the EPT on temperature and humidity, the RAOBs/NUCAPS differences in these parameters are affecting the accuracy of the NUCAPS EPT, and consequently, of the NUCAPS GDI. Given the critical dependence of the final EPT upon the latent heat released during the pseudo adiabatic ascent (used to warm the lifting air parcel), the magnitude of NUCAPS EPT differences in relation to RAOBs must increase in warm humid atmospheric conditions. In this case, the drier NUCAPS derived parcels (resulting from the NUCAPS water vapor negative biases found for the four levels used during GDI computation) produce lower EPTs than the ones produced by RAOBs, and larger RAOBs/NUCAPS EPT differences in comparison with drier environments. On the contrary, in drier conditions, the contribution of the latent heat release to the EPT is less important since air parcels contain less moisture. This means that the negative biases found for NUCAPS water vapor become a less significant source of error for the final NUCAPS EPT, resulting in smaller RAOBs/NUCAPS differences. The previous discussion helps to understand the behavior of GDI values higher than about 30 (RAOBs defined), in which NUCAPS GDI tend to be underestimates of RAOBs GDI. From its definition, GDI above 30 typically occurs in warm humid convectively unstable environments (free of inhibiting factors for convective weather, such as subsidence inversions and mid-levels ridges). Nonetheless, relatively few cases (less than 2%, as shown in Fig. 8) in this category occurred, which can be playing a role in limiting the evaluation of NUCAPS GDI skill under such cases.

6.2 Referende/Dedicated Radiosondes

Figures 9 and 10 show the validation results for NUCAPS SIPs, using dedicated/reference radiosondes as the truth measurements (mid-latitudes). As previously mentioned, dedicated/reference radiosondes constitute an entirely independent dataset (not assimilated in NWP models), with optimum quality and synchronized with satellite observations. As can be verified from results presented in Figures 9 and 10, the NUCAPS SIPs shows similar characteristics and performance than the assessment found in previous section, helping to support the major conclusion obtained when conventional RAOBs were used. In this respect, it is verified that, for the range of SIPs values associated with unstable atmospheric conditions, and computed using RAOBs, NUCAPS SIPs tend to underestimate those conditions. It is also important to highlight the overall reduction in the statistical errors for NUCAPS and ECMWF with respect to the ones reported for conventional RAOBs. This behavior can be explained by the reduction of the collocation error and the better error characterization of the reference/dedicated RAOBs, which produce higher quality RAOB measurements. These properties are part of the major justification and value of using dedicated/reference observations for the validation of the NUCAPS EDRs, which now is being extended to the validation of the NUCAPS SIPs.
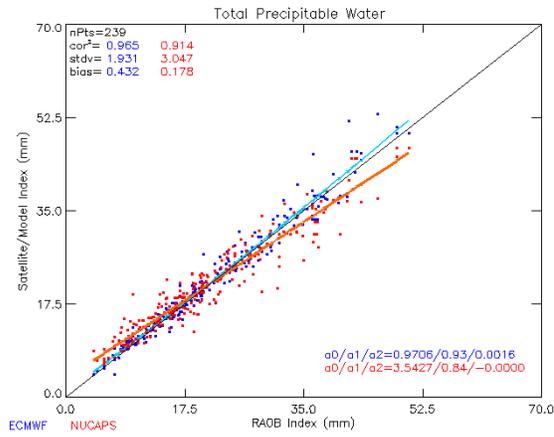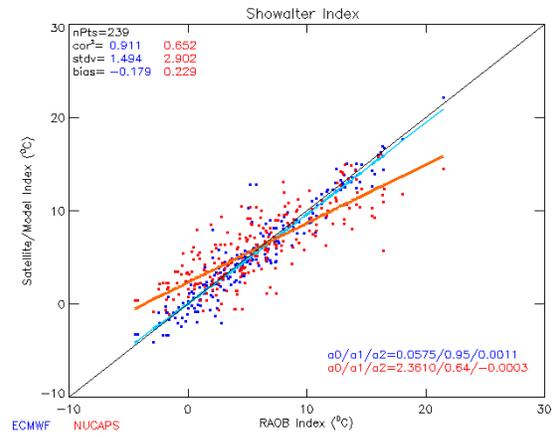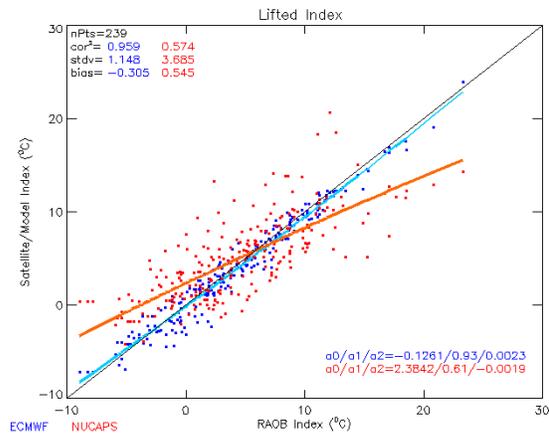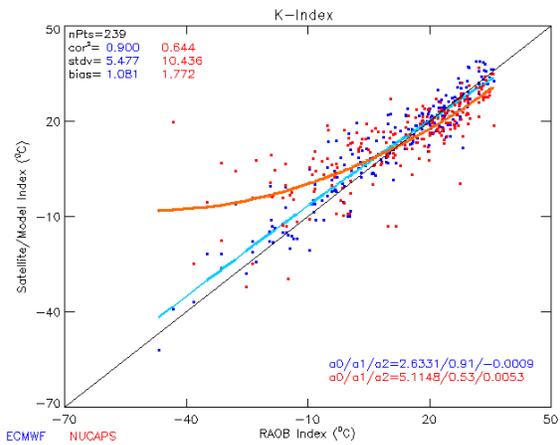
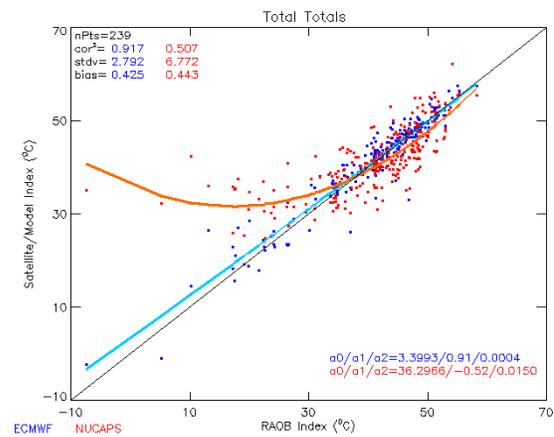Figure 9. Scatter plots of dedicated/reference RAOBs versus NUCAPS/ECMWF versions of (a) TPW; (b) SWI; (c) LI; (d) KI; and (e) TT for mid-latitudes.
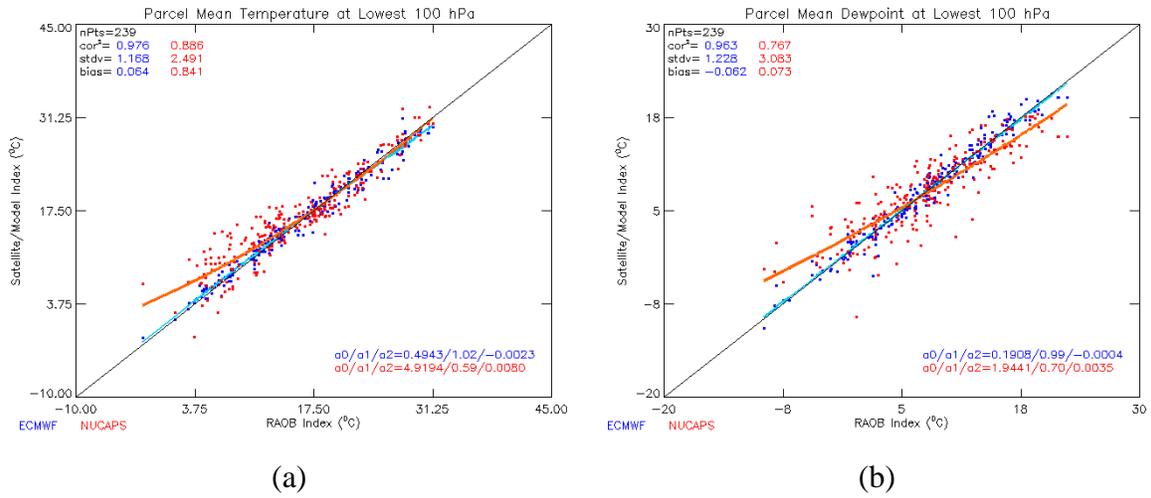
Figure 10. Scatter plots of dedicated/reference RAOBs versus NUCAPS/ECMWF versions of (a) Parcel Mean Temperature at Lowest 100 hPa; and (b) Parcel Mean Dewpoint at Lowest 100 hPa.

59

Chapter 7. Case Studies

This chapter presents two case studies in order to demonstrate the area of application and possible operational usage of the NUCAPS-derived SIPs. ECMWF analyses are employed as baselines for comparisons. Since ECMWF analyses are available with a frequency of 6 hours per day at a regular grid-spacing, it was necessary to perform a 4-point spatiotemporal interpolation to match NUCAPS time and locations of retrievals.

It is important to mention that the nature of the sun-synchronous S-NPP satellite with its ascending and descending orbits crossing the equator at approximately 1330 and 0130 local time (LT), respectively, determines the satellite passage times over the continental US (CONUS), and the availability of NUCAPS products. More specifically, the S-NPP overpasses (in ascending mode) over the CONUS occur from the east to the west direction between about 1700 and 2300 Universal Coordinated Time (UTC).

7.1 08 May 2015

During the afternoon of 08 May 2015, multi-cellular convective storms developed over the south-central states of the US, resulting in multiple reports of severe weather (tornados, high winds and large hails) (Fig. 11).
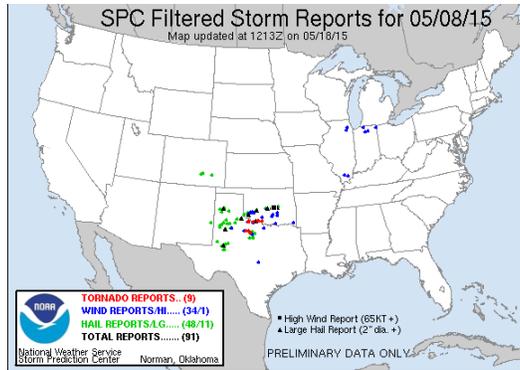
Figure 11. Filtered Storm reports product for 08 May 2015. Product covers the period between 08 May 1200 and 09 May 1159 UTC. (Courtesy of the NOAA/Storm Prediction Center (SPC). Available online at www.spc.noaa.gov/climo/reports/150508_rpts.html.)

Strong to severe thunderstorms evolved in the warmer, moist and unstable environment ahead of a surface cold front (Fig. 12). Persistent low-level southerly winds provided the inflow of warm moist air from the Gulf of Mexico into the region throughout the day. The dryline at the surface analysis map indicates the boundary between the warm moist air ahead (dewpoints reaching the lower 70's F) and the drier continental air mass behind it.
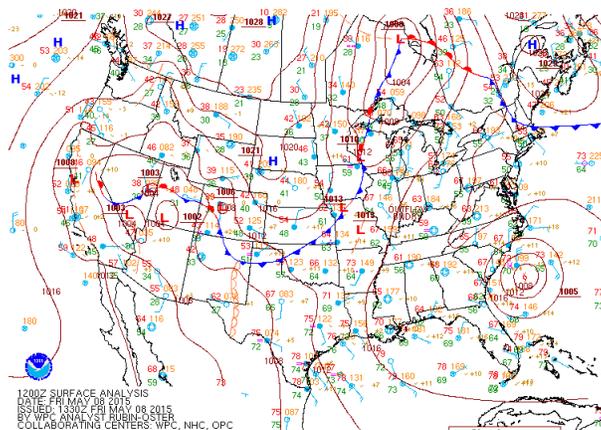

Figure 12. 1200 UTC surface analysis map for 08 May 2015. (Courtesy of the NOAA/NCEP/Weather Prediction Center (WPC). Available online at http://www.wpc.ncep.noaa.gov/archives/web_pages/sfc/sfc_archive.php.)

61

The GOES-13 IR images (Fig. 13) show the development of the convective cells over the focus area on that day (Fig. 13c refers to the closest time to the NPP ascending passage over the region).
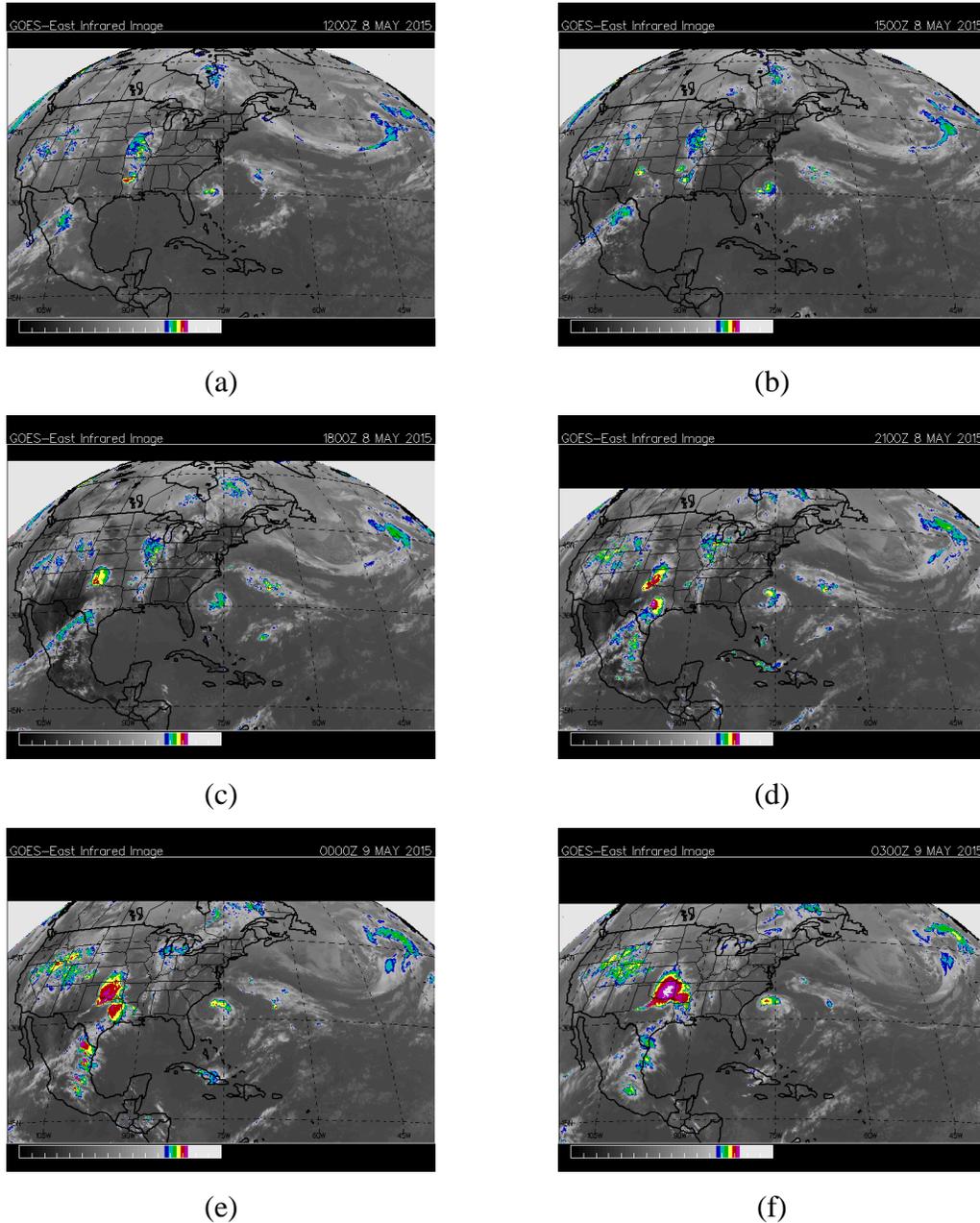

Figure 13. GOES-13 IR images from 1200 UTC 08 May 2015 to 0300 UTC 09 May 2015. Sequence covers (a) 1200 UTC; (b) 1500 UTC; (c) 1800 UTC; (d) 2100 UTC; (e) 0000 UTC; and (f) 0300 UTC. (Courtesy of the San Francisco State University. Available online at http://squall.sfsu.edu/crws/archive/satimgs_month_arch.html.)

Figure 14 shows the comparison of NUCAPS TPW, LI and TT maps against the corresponding ECMWF products, considering the S-NPP ascending passage of 08 May 2015. It is evident that there is a high level of agreement between NUCAPS TPW and ECMWF TPW. NUCAPS TPW is able to identify the regions with the largest supply of moisture in the atmospheric column, especially over the south-central US. In comparison with the ECMWF products, NUCAPS LI and TT show an overall good agreement. Both NUCAPS products can distinguish zones with stable atmospheric conditions from the areas of strong instability. There is a clear transition from the most stable to the unstable zones, despite differences verified in some areas. For example, NUCAPS TT appears somewhat underestimated in the northeast US, for example around Indiana, and NUCAPS LI reveals increased instability over parts of the southeastern US. Of more relevance in the context of the case study selected is that the unstable atmospheric conditions over the south-central US were captured by both NUCAPS products. The agreement between ECMWF and NUCAPS over large regions, demonstrates that NUCAPS SIPs can help forecasters to identify areas under unstable atmospheric conditions that can result in strong convective development within the next few hours.

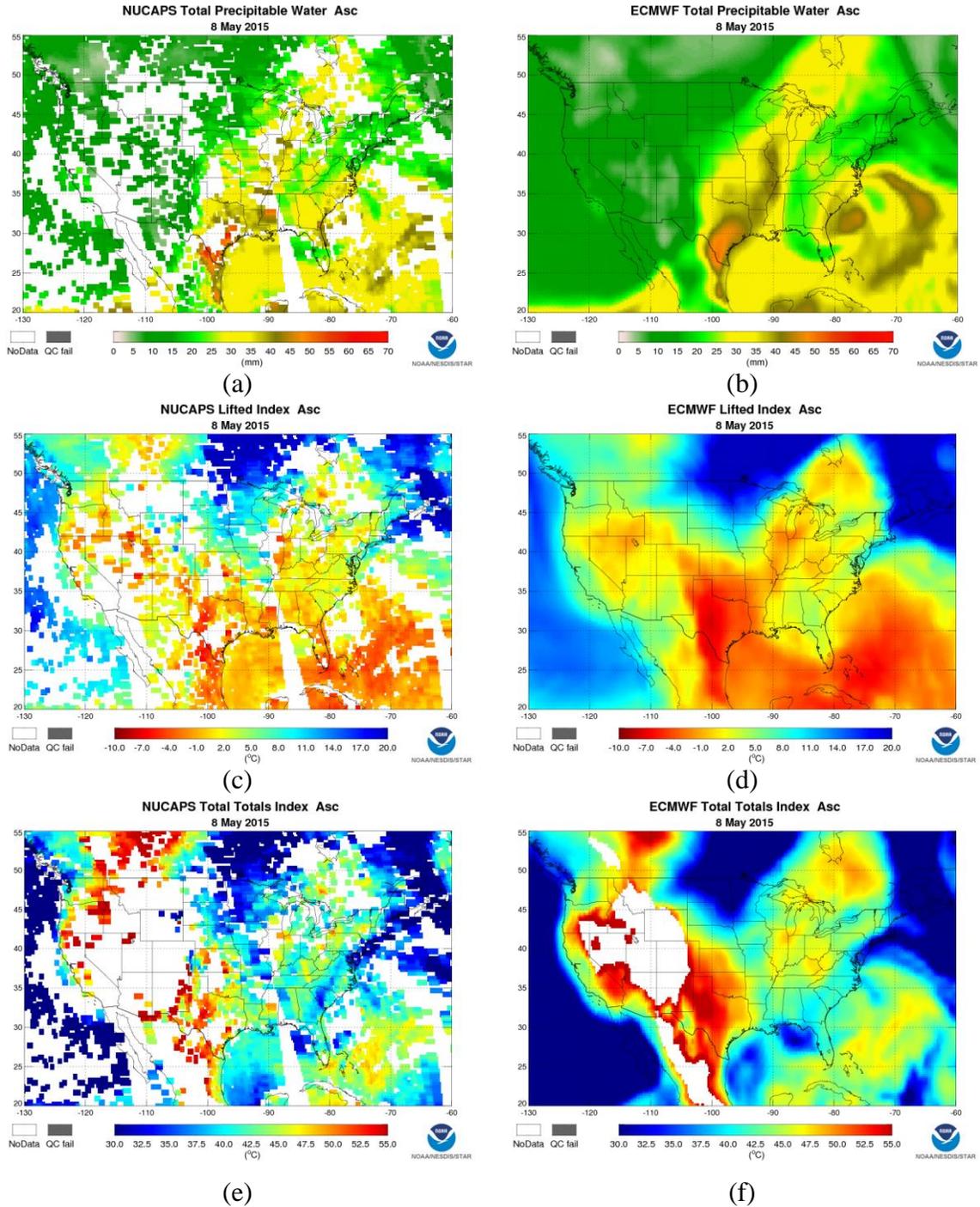Figure 14. NUCAPS derived fields of (a) TPW; (c) LI; and (e) TT compared with ECMWF derived maps of (b) TPW; (d) LI; and (f) TT for 08 May 2015 in ascending node. High-elevated areas where TT is undefined appear in blank (see the ECMWF map for a prompt identification). Note that areas where the NUCAPS algorithm failed are also shown in blank (they should be distinguished from the satellite orbital gaps).

To complement the evaluation, KI and SWI maps are presented in Figure 15, although both indices were not specifically developed to measure the likelihood of severe convection development. It can be seen that NUCAPS KI and SWI fields compare reasonably well with ECMWF, since NUCAPS is capable of reproducing similar atmospheric stability patterns to the ones estimated by ECMWF.

(a)   (b)

(c)   (d)

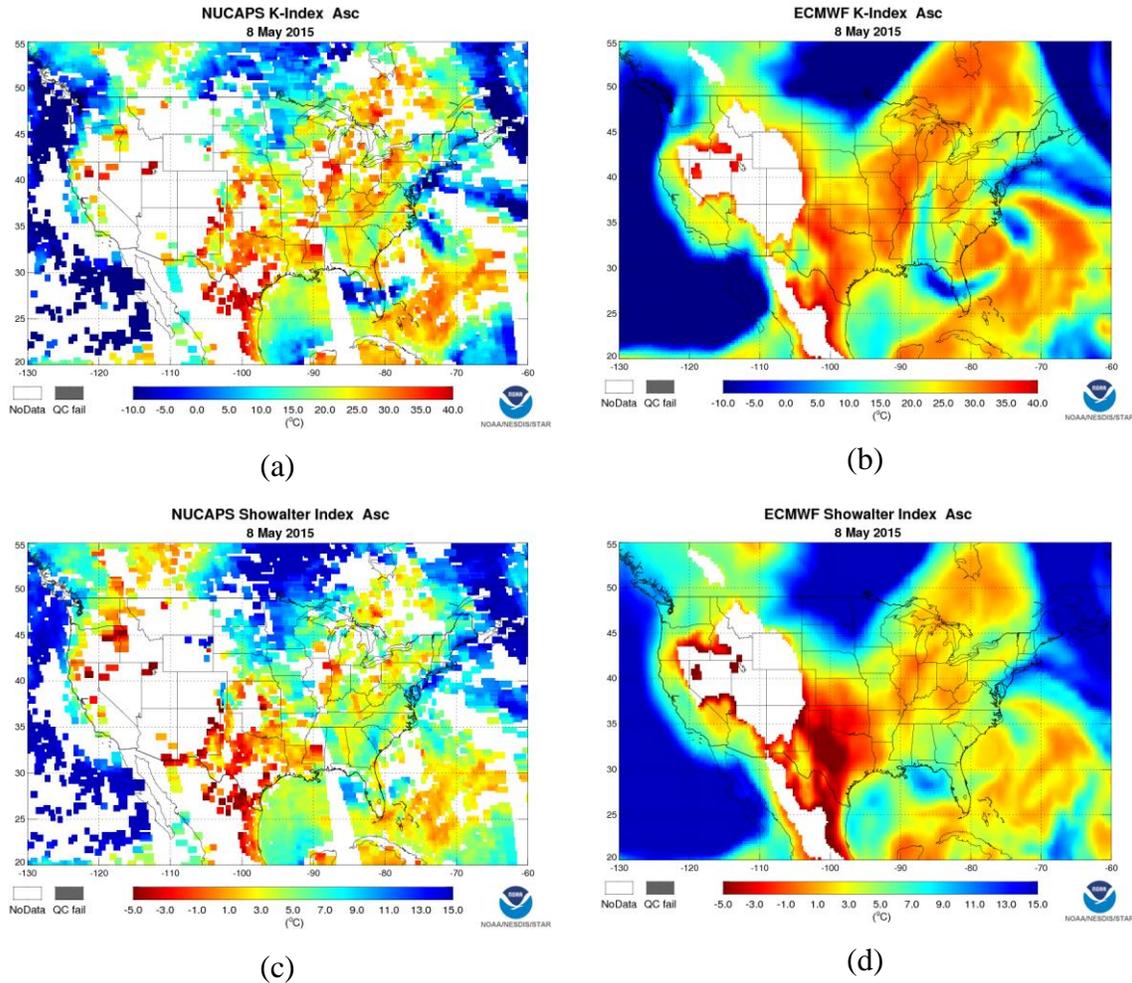Figure 15. NUCAPS derived fields of (a) KI; and (c) SWI compared with ECMWF derived maps of (b) KI; and (d) SWI for 08 May 2015 in ascending node. High-elevated areas where KI and SWI are undefined appear in blank (see the ECMWF map for a prompt identification). Note that areas where the NUCAPS algorithm failed are also shown in blank (they should be distinguished from the satellite orbital gaps).

7.2 25 May 2015

In the following, the same applicability of NUCAPS SIPs is demonstrated for the episode of 25 May 2015. This case, presented more concisely below, was marked by strong convective development over the states of Texas, Oklahoma, Arkansas, Louisiana and Mississippi (see Fig. 16), which caused severe weather occurrence with significant socio-economic impacts (Fig. 17).

(a)   (b)

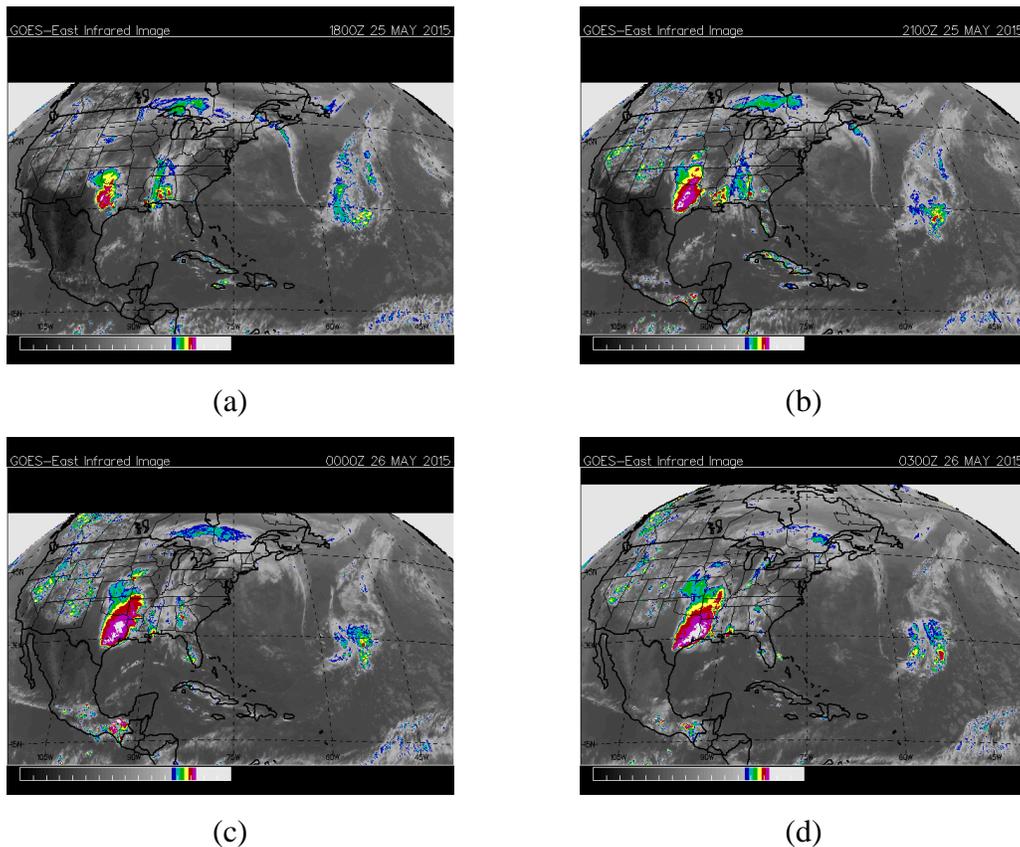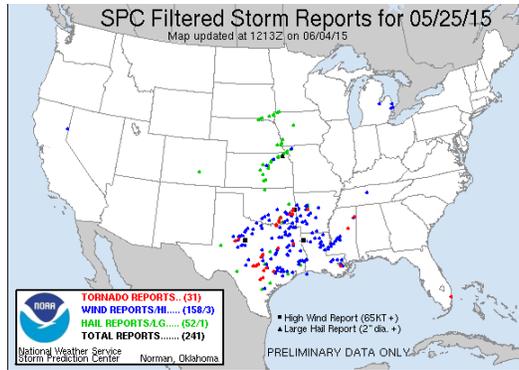(c)   (d)

Figure 16. GOES-13 IR images from 1800 UTC 25 May 2015 to 0300 UTC 26 May 2015. Sequence covers (a) 1800 UTC; (b) 2100 UTC; (c) 0000 UTC; and (d) 0300 UTC. (Courtesy of the San Francisco State University. Available online at http://squall.sfsu.edu/crws/archive/satimgs_month_arch.html.)

(e)

Figure 17. Filtered Storm reports product for 25 May 2015. Product covers the period between 25 May 1200 and 26 May 1159 UTC. (Courtesy of the NOAA/Storm Prediction Center (SPC). Available online at www.spc.noaa.gov/climo/reports/250508_rpts.html.)

Like the previous case, NUCAPS TPW, LI and TT compare favorably against their ECMWF versions (Fig. 18). Apart from the high instability over the aforementioned US States, NUCAPS SIPs were also able to capture the unstable signature over the central portion of the US. Deep convection over this area produced large hail in the States of Kansas, Nebraska, South Dakota, Iowa and Missouri (see Fig. 17), which occurred between approximately 252000 and 260100 UTC (source: http://www.spc.noaa.gov/climo/reports/150525_rpts.html).

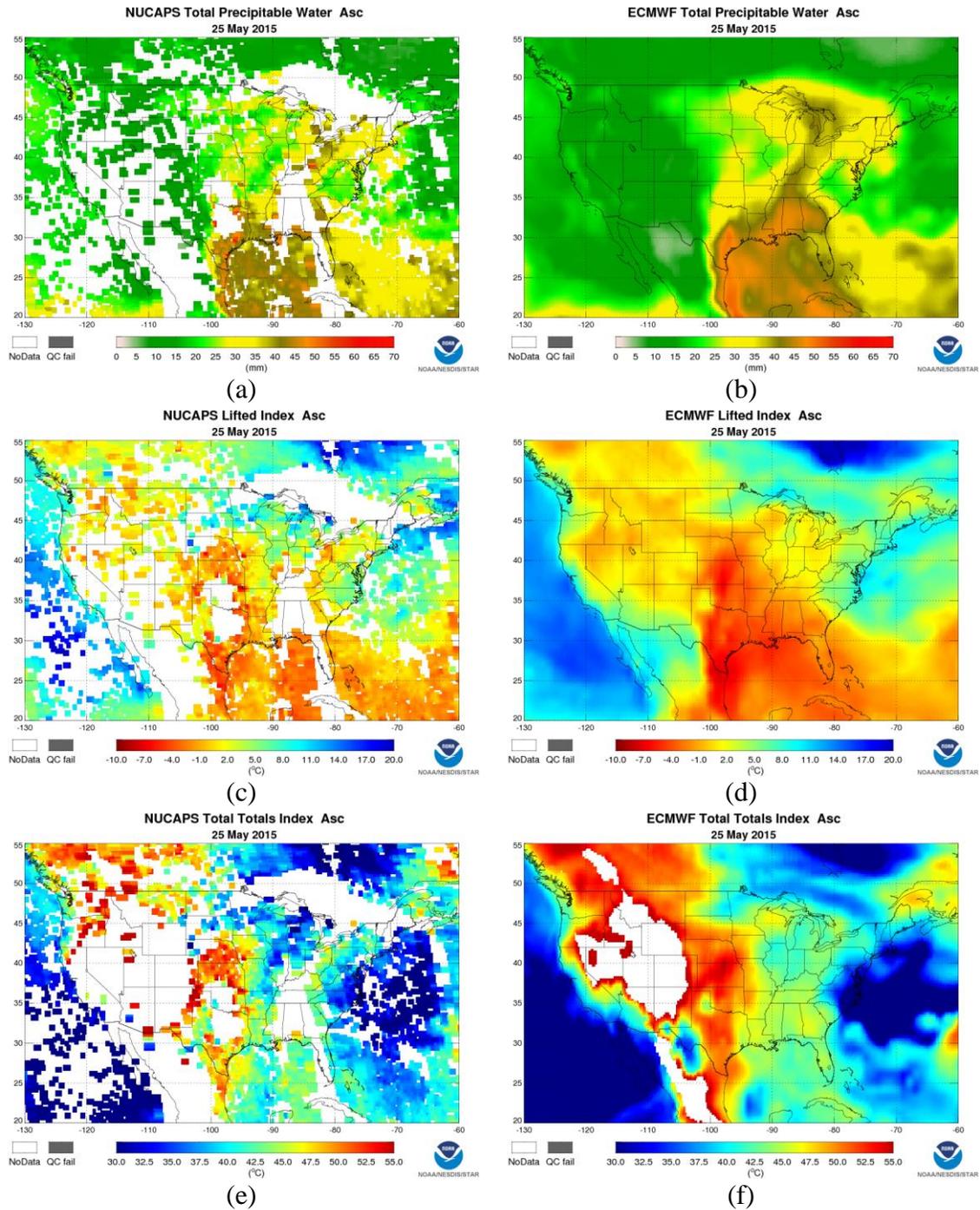Figure 18. NUCAPS derived fields of (a) TPW; (c) LI; and (e) TT compared with ECMWF derived maps of (b) TPW; (d) LI; and (f) TT for 25 May 2015 in ascending node. High-elevated areas where TT is undefined appear in blank (see the ECMWF map for a prompt identification). Note that areas where the NUCAPS algorithm failed are also shown in blank (they should be distinguished from the satellite orbital gaps).

Chapter 8. Summary and Conclusions

This work demonstrated, through objective and qualitative comparisons against ground-based RAOBs and ECMWF numerical outputs, that the NUCAPS derived SIPs constitute complementary and useful products for the evaluation of the static/convective stability of the atmosphere, best suited for synoptic-scale applications.

Among all SIPs evaluated, NUCAPS TPW exhibited the highest level of statistical agreement with RAOB counterparts over both latitudinal bands. The remaining SIPs (SWI, LI, KI, TT and GDI) exhibited good to intermediate levels of agreement with their RAOBs derived versions, with the caveat that these parameters tended to be underestimates of RAOBs, particularly over the range of values associated with unstable atmospheric conditions. Main reasons behind this result are: the cold BIAS at/nearby the surface level below a warm BIAS layer (increasing the static stability of the atmosphere); and the dry BIAS present in whole tropospheric column, as verified in Chapter 5. Therefore, in order to further improve the quality of the NUCAPS-derived SIPs, an improvement in the accuracy and horizontal resolution of the retrieved AVTPs and AVMPs is required.

The comparison results over severe weather cases demonstrated that NUCAPS has the capability of generating reliable fields of atmospheric stability, identifying areas under unstable atmospheric conditions, as well as capturing synoptic-scale convective signatures.

Limitations on the accuracy of the NUCAPS retrievals are mainly caused by clouds contamination and areas under precipitation, in which NUCAPS is unable to

converge to a solution. On the other hand, when the profile is obtained over partly cloudy/cloudy scenes, the quality of the products is degraded since the cloud clearing module can also introduce errors. Moreover, the poorer NUCAPS representation of the near surface temperature and moisture conditions represents another restricting factor.

The immediate application of this work is to benefit current and potential users of the NUCAPS AVTPs/AVMPs and stability products. In this regard, NUCAPS soundings and some stability products have been progressively implemented as part of the AWIPS-II forecasting software, which is the operational display and analysis package in use by the National Weather Service (NWS). This work is expected to provide objective information about the performance of NUCAPS products and serve as a benchmark for the analysis performed by operational forecasters at many NWS offices nationwide.

Of high value is the availability of the AVTPs and AVMPs products in the early afternoon at many US states, a critical time for the evaluation of the thermodynamic conditions of the atmosphere and its potential for the initiation of convection. Thermodynamic profiles are unavailable at this time since operational RAOBs are launched twice a day, one at 00 and another at 12 UTC. In addition to that, the global limitations on the spatial RAOBs coverage should also be considered, since this is far from the ideal even in the US, where rawinsonde locations can be up to a few hundreds of kilometers apart. In this respect, an additional benefit from the use of NUCAPS stability products in the developing countries is expected, where RAOBs are extremely limited or even absent. Moreover, increased temporal coverage of NUCAPS soundings can be obtained through a constellation of platforms from the JPSS, Aqua EOS and MetOp

missions due to the modular nature of the code. As described before, NUCAPS can use input measurements from multiple current (and future) IR/MW suites of sensors.

In this work, no attempt was made to partition the analyses among clear-sky, partly-cloudy and cloudy conditions. This will be object of future work. Given the known fact that satellite-observed IR radiances are contaminated by clouds (requiring cloud clearing algorithms), it is expected that the optimum performance of the NUCAPS derived SIPs occur in cloud-free areas. In this case, the analysis of pre-convective environments prior to the formation of cumulus clouds and deep convection constitutes the most suitable scenario of application of NUCAPS derived stability products.

The operational application of the NUCAPS soundings and derived SIPs is not intended to replace RAOBs use. Satellite retrievals are unable to achieve the same vertical resolution of the radiosonde profiles, which means that the finest details and changes in the thermodynamic profile are not resolved. Hence it is expected that the forecasters make use of such products in combination with other observational data and analysis tools (e.g., numerical outputs) for the identification of mechanisms that may trigger deep convection and closely monitoring. Under this perspective, NUCAPS stability products are proposed to be complementary tools for nowcasting applications.

This work represents the initial evaluation and foundation of the atmospheric stability products generated by observations from the JPSS series. All points addressed here aim to establishing a larger inquiry into the full capability of NUCAPS soundings and stability products, which is far from completely explored.

Future work involves the evaluation of the NUCAPS version of the Convective Available Potential Energy (CAPE), a parameter widely used on the operational forecasting environment. Further research is planned to extend this evaluation to include NUCAPS derived SIPs based on measurements of the MetOp-B satellite.

References

Bauer, P., A. Thorpe, and G. Brunet., 2015: The quiet revolution of numerical weather prediction. Nature 525, 47-55, doi:10.1038/nature14956.

Bolton, D., 1980: The Computation of Equivalent Potential Temperature. Monthly Weather Review, 108, 1046–1053, doi:10.1175/1520-0493(1980)108<1046:TCOEPT>2.0.CO;2.

Bryan, G. H., 2008: On the Computation of Pseudoadiabatic Entropy and Equivalent Potential Temperature. Monthly Weather Review, 136, 5239-5245, doi:10.1175/2008MWR2593.1.

Candlish, L. M., R. L. Raddatz, M. G. Asplin, and D. G. Barber, 2012: Atmospheric Temperature and Absolute Humidity Profiles over the Beaufort Sea and Amundsen Gulf from a Microwave Radiometer. J. Atmos. Oceanic Technol., 29, 9, 1182-1201, doi:10.1175/JTECH-D-10-05050.1.

Chahine, M. T., 1974: Remote Sounding of Cloudy Atmospheres. I. The Single Cloud Layer. Journal of the Atmospheric Sciences, 31(1), 233-243, doi:10.1175/1520-0469(1974)031<0233:rsocai>2.0.co;2.

Chesters, D., A. Mostek, and D. A. Keyser, 1986: VAS sounding images of atmospheric stability parameters. Weather Forecast., 1, 5–22, doi:10.1175/1520-0434(1986)001<0005:VSIOAS>2.0.CO;2.

Craven, J. P., R. E. Jewell, and H. E. Brooks, 2002: Comparison between observed convective cloud base heights and lifting condensation level for two different lifted parcels. Wea. Forecasting, 17, 4, 885-890.

Davies-Jones, R., 2009: On Formulas for Equivalent Potential Temperature. Monthly Weather Review, 137, 3137-3148, doi:10.1175/2009MWR2774.1.

Dostalek, J. F., and T. J. Schmit, 2001: Total precipitable water measurements from GOES Sounder derived product imagery. Wea. Forecasting, 16, 573–587.

Doswell, C. A., J. T. Schaefer, D. W. McCann, T. W. Schlatter, and H. B. Wobus, 1982: Thermodynamic analysis procedures at the National Severe Storms Forecast Center. Preprints, Ninth Conf. on Weather Forecasting and Analysis, Seattle, WA, Amer. Meteor. Soc., 304–309.

Galvez, J. M., and M. Davison, 2014: The Galvez-Davison Index for Tropical Convection. Preprints, 26th Conference on Weather Analysis and Forecasting / 22nd Conference on Numerical Weather Prediction. Amer. Meteor. Soc., Atlanta, Georgia, February 1-6.

Galway, J. G., 1956: The lifted index as a predictor of latent instability. Bull. Amer. Meteor. Soc., 37, 528–529.

Gambacorta, A., and C. D. Barnet, 2013: Methodology and Information Content of the NOAA NESDIS Operational Channel Selection for the Cross-Track Infrared Sounder (CrIS). IEEE Transactions on Geoscience and Remote Sensing, vol. 51, no. 6, pp. 3207-3216, June 2013, doi: 10.1109/TGRS.2012.2220369.

Gambacorta, A., *et al*., 2014: An Experiment Using High Spectral Resolution CrIS Measurements for Atmospheric Trace Gases: Carbon Monoxide Retrieval Impact Study. IEEE Geoscience and Remote Sensing Letters, vol. 11, no. 9, pp. 1639-1643, doi: 10.1109/LGRS.2014.2303641.

George, J. J., 1960: Weather Forecasting for Aeronautics. Academic Press, 673 pp.

Goldberg, M. D., Qu, Y. N., McMillin, L. M., Wolf, W., Zhou, L. H., & Divakarla, M., 2003: AIRS near-Real-Time Products and Algorithms in Support of Operational Numerical Weather Prediction. IEEE Transactions on Geoscience and Remote Sensing, 41(2), 379-389, doi:10.1109/tgrs.2002.808307.

Goldberg, M. D., H. Kilcoyne, H. Cikanek, and A. Mehta, 2013: Joint Polar Satellite System: The United States next generation civilian polar-orbiting environmental satellite system. J. Geo phys. Res. Atmos., 118, 13,463–13,475, doi:10.1002/2013JD020389.

Haklander, A. J., and A. Van Delden, 2003: Thunderstorm predictors and their forecast skill for the Netherlands. Atmos. Res., 67–68, 273–299.

Han, Y., *et al.*, 2013: Suomi NPP CrIS measurements, sensor data record algorithm, calibration and validation activities, and record data quality. J. Geophys. Res. Atmos., 118, 12,734–12,748, doi:10.1002/2013JD020344.

Hayden, C. M., 1988: GOES-VAS simultaneous temperature–moisture retrieval algorithm. J. Appl. Meteor., 27, 705–733.

Johns, R. H., and C. A. Doswell, 1992: Severe Local Storms Forecasting. Wea. Forecasting, 7, 588–612. doi:10.1175/1520-0434(1992)007<0588:SLSF>2.0.CO;2.

Koenig, M., and E. De Coning, 2009: The MSG Global Instability Indices Product and Its Use as a Nowcasting Tool. Wea. Forecasting, 24, 272–285, doi:10.1175/2008WAF2222141.1.

Lee, F., *et al.*, 2010: NPOESS: Next-Generation Operational Global Earth Observations.
Bull. Am. Meteorol. Soc., 91, 727–740, doi:10.1175/2009BAMS2953.1.

Li, Z., J. Li, W. P. Menzel, T. J. Schmit, J. P. Nelson III, J. Daniels, and S. A. Ackerman,
2008: GOES sounding improvement and applications to severe storm nowcasting.
Geophys. Res. Lett., 35, L03806, doi:10.1029/2007GL032797.

Li, Z., J. Li, W. P. Menzel, J. P. Nelson III, T. J. Schmit, E. Weisz, and S. A. Ackerman,
2009: Forecasting and nowcasting improvement in cloudy regions with high
temporal GOES sounder infrared radiance measurements. J. Geophys. Res., 114,
D09216, doi:10.1029/2008JD010596.

Menzel, W. P., F. C. Holt, T. J. Schmit, R. M. Aune, A. J. Schreiner, G. S. Wade, and D.
G. Gray, 1998: Application of GOES-8/9 soundings to weather forecasting and
nowcasting. Bull. Amer. Meteor. Soc., 79(10), 2059–2077, doi:10.1175/1520-
0477(1998)079<2059:AOGSTW>2.0.CO;2.

Miller, R. C, 1967: Notes on analysis and severe storm forecasting procedures of the
Military Weather Warning Center. Tech. Report 200(R), AWS, USAF, 94 pp.
[Headquarters, AWS, Scott AFB, IL 62225]

Mostek, A., L. W. Uccellini, R. A. Petersen, and D. Chesters, 1986: Assessment of VAS
soundings in the analysis of a pre-convective environment. Mon. Weather Rev.,
114, 62–87, doi:10.1175/1520-0493(1986)114<0062:AOVSIT>2.0.CO;2.

Nalli, N. R., *et al.*, 2011: Multi-year observations of the tropical Atlantic atmosphere:
Multidisciplinary applications of the NOAA Aerosols and Ocean Science

Expeditions (AEROSE). Bull. Am. Meteorol. Soc., 92, 765–789, doi: 0.1175/2011BAMS2997.1.

Nalli, N. R., *et al.*, 2013: Validation of satellite sounder environmental data records: Application to the Cross-track Infrared Microwave Sounder Suite. J. Geophys. Res. Atmos., 118, 13,628–13,643, doi:10.1002/2013JD020436.

Peppler, R. A., 1988: A review of static stability indices and related thermodynamic parameters. SWS Misc. Publ. 104, Illinois State Water Survey Division, Climate and Meteorology Section, 94 pp.

Peppler, R. A., and P. J. Lamb, 1989: Tropospheric static stability and central North American growing season rainfall. Mon. Wea. Rev., 117, 1156–1180.

Reale, T., B. Sun, F. H. Tilley, M. Pettey, 2012: The NOAA Products Validation System (NPROVS). J. Atmos. Oceanic Technol., 29, 629–645, doi:10.1175/JTECH-D-11-00072.1.

Rosenkranz, P. W., 2001: Retrieval of Temperature and Moisture Profiles from AMSU-A and AMSU-B Measurements. IEEE Transactions on Geoscience and Remote Sensing, 39(11), 2429-2435, doi:10.1109/36.964979.

Schmit, T. J., W. F. Feltz, W. P. Menzel, J. Jung, A. P. Noel, J. N. Heil, J. P. Nelson III, and G. S. Wade, 2002: Validation and use of GOES sounder moisture information. Weather Forecast., 17(1), 139–154, doi:10.1175/1520-0434(2002)017<0139:VAUOGS>2.0.CO;2.

Simmons, A. J., and Hollingsworth, A., 2002: Some aspects of the improvement in skill of numerical weather prediction. Q. J. R. Meteorol. Soc., 128: 647–677, doi: 10.1256/003590002321042135.

Smith, W. L., G. S. Wade, and H. M. Woolf, 1985: Combined Atmospheric Sounding/Cloud Imagery—A New Forecasting Tool. Bull. Amer. Meteor. Soc., 66, 138–141.

Smith, W. L., *et al.*, 2009: Technical note: Evolution, current capabilities, and future advance in satellite nadir viewing ultraspectral IR sounding of the lower atmosphere. Atmos. Chem. Phys, 9, 5563–5574, doi:10.5194/acp-9-5563-2009.

Smith, N., W. L. Smith, E. Weisz, and H. E. Revercomb, 2015: AIRS, IASI, and CrIS Retrieval Records at Climate Scales: An Investigation into the Propagation of Systematic Uncertainty. J. Appl. Meteor. Climatol., 54(7), 1465-1481, doi: 10.1175/JAMC-D-14-0299.1.

Showalter, A. K., 1953: A stability index for thunderstorm forecasting. Bull. Amer. Meteor. Soc., 34, 250-252.

Susskind, J., C. D. Barnet, and J. M. Blaisdell, 2003: Retrieval of Atmospheric and Surface Parameters from AIRS/AMSU/HSB data in the presence of clouds. IEEE Trans. Geosci. Remote Sens., 41(2), 390–409, doi:10.1109/TGRS.2002.808236.

Susskind, J., J. Blaisdell, L. Iredell, and F. Keita, 2011: Improved temperature sounding and quality control methodology using AIRS/AMSU data: The AIRS science team version 5 retrieval algorithm, IEEE Trans. Geosci. Remote Sens., 49(3), 883–907, doi:10.1109/TGRS.2010.2070508.

Tan, C., *et al*., 2015: The Preprocessor of the NOAA Unique CRIS/ATMS Processing System (NUCAPS). STAR JPSS Annual Science Team Meeting, August 25, 2015, College Park, MD. [Online]. Available: http://www.star.nesdis.noaa.gov/star/documents/meetings/2015JPSSAnnual/Posters/05_PosterI_Tan.pdf

Tobin, D., *et al.*, 2013: Suomi-NPP CrIS radiometric calibration uncertainty. J. Geophys. Res. Atmos., 118, 10,589–10,600, doi:10.1002/jgrd.50809.

Wallace, J. M., and P. V. Hobbs, 2006: Atmospheric Science: An Introductory Survey, 2nd edition, Academic Press, 504 pp.

Weng, F., X. Zou, X. Wang, S. Yang, and M. D. Goldberg, 2012: Introduction to Suomi National Polar-Orbiting Partnership advanced technology microwave sounder for numerical weather prediction and tropical cyclone applications. J. Geophys. Res., 117, D19112, doi:10.1029/2012JD018144.

Weng, F., X. Zou, N. Sun, H. Yang, M. Tian, W. J. Blackwell, X. Wang, L. Lin, and K. Anderson, 2013: Calibration of Suomi national polar-orbiting partnership advanced technology microwave sounder. J. Geophys. Res. Atmos., 118, 11,187–11,200, doi:10.1002/jgrd.50840.

Wilks, D. S., 2011: Statistical Methods in the Atmospheric Sciences, 3rd edition, Academic Press, 676 pp.

Zavyalov, V., *et al.*, 2013: Noise performance of the CrIS instrument. J. Geophys. Res. Atmos.*,* 118*,* 13,108–13,120, doi:10.1002/2013JD020457.

Zou, X., L. Lin, and F. Weng, 2013: Absolute calibration of ATMS upper level temperature sounding channels using GPS RO observations, IEEE Trans. Geosci. Remote Sens., PP(99), 1, doi:10.1109/TGRS.2013.2250981.